DE90004019

CIRCULATION IN GAS-SLURRY COLUMN REACTORS: SEVENTH QUARTERLY REPORT, QUARTER ENDING JUNE 30, 1989

WEST VIRGINIA UNIV., MORGANTOWN. DEPT.
OF MECHANICAL AND AEROSPACE ENGINEERING

1989

U.S. Department of Commerce
National Technical Information Service

DE90004019

LEGIBILITY NOTICE

A major purpose of the Technical Information Center is to provide the broadest dissemination possible of information contained in DOE's Research and Development Reports to business, industry, the academic community, and federal, state and local governments.

Although a small portion of this report is not reproducible, it is being made available to expedite the availability of information on the research discussed herein.

DE90004019

DOE/PC/79935--12

DE90 004019

"CIRCULATION IN GAS-SLURRY COLUMN REACTORS"
DEPARTMENT OF ENERGY. CONTRACT NUMBER DE-FG22-87PC79935
SEVENTH QUARTERLY REPORT - REPORT DOE/PC/79935-12

QUARTER ENDING 6/30/89

Prepared by
West Virginia University
Department of Mechanical and Aerospace Engineering

Principal Investigators
Nigel Clark
John Kuhlman
Ismail Celik

Prepared for
DEPARTMENT OF ENERGY, PITTSBURGH

CONTENTS

1. INTRODUCTION

During this quarter progress has been made in all 3 areas of the bubble column research (probe measurements, laser doppler anemometry and numerical modeling of the two phase flow). In particular, bubble velocities can now be inferred from cross-correlation of two probe signals, and the numerical modeling has yielded circulation streamlines for a bubble column in laminar flow. Liquid velocities can also be measured in a hexagonal test column with the laser doppler velocimeter. Details of this research progress follow.

2. RESISTANCE PROBE MEASUREMENTS

The bulk of the air-water void profile data gathering is now complete, with profiles available for two traverses (at right angles to one another) at varying heights of mixture in the column. Data has been taken at several different heights and different air flowrates in each column. Figures 2.1 to 2.6 provide data on the column containing an unaerated water height of 12 inches. Figures 2.7 to 2.18 present data for the unaerated water height of 24 inches and Figures 2.19 to 2.27 give an incomplete data set for the case of an unaerated water height of 36 inches. Note that the voidage distribution is initially relatively uniform versus radius near the bottom of the column, but becomes more non-uniform as the top of the column is approached. Voidage is highest on the centerline. These data indicate that the initial uniform injection of bubbles at the distributor plate is altered by an inwards migration of bubbles towards the centerline of the column as they rise up the column.

In addition, hardware and software has been developed to infer vertical bubble velocities in the column. This is achieved by cross-correlating the two voltage signals from two separate resistance probe tips, the one tip being located directly above the other. A probe with vertical tip spacing of 3/8 inch (as shown in Figure 2.28) has been manufactured, and the two tips have been tested separately in air and water. Data is sampled rapidly (at 2000 Hz) from the probes, and stored in computer memory. The two signals are then cross-correlated to find the best-fit time lag between bubbles reaching the lower probe and the same bubbles reaching the upper probe. A copy of the cross-correlation program is attached to this report in Appendix A. Figure 2.29 shows high resolution traces of voltage from the upper and lower probes on the same set of axes. The troughs in each trace indicate bubble presence, and the time delay between traces is evident. The accuracy of the cross-correlation scheme and the probe hardware has been determined by placing the probes in a stream of bubbles rising from a point source below the probes. One would expect the measured velocity of this string of bubbles to be slightly greater than the rise velocity of a lone bubble in water, which is known to be about 240 mm/sec. for bubbles of size between the Stokes and bubble cap regimes. The program showed a satisfactory rise velocity of 255 mm/sec. It can now be used with confidence to find the bubble velocity in circulating systems. These bubble velocities can then be compared with the liquid velocities predicted by the numerical modeling, and by the one-dimensional models discussed previously in this research. The one-dimensional model has recently been checked for this purpose, and some processed data are already available. Figure 2.30 shows the shear-stress profile associated with the void fraction distribution and mean local density distribution shown in Figures 2.31 and 2.32 respectively. Figure 2.33 shows the liquid velocity distribution predicted from the shear stress distribution using water viscosity and a Prandtl mixing length approach. Figure 2.34 shows three predicted liquid velocity profiles arising from actual void data taken in the column. This will be compared with bubble velocity data acquired from the column during the next quarter.

3. LASER DOPPLER VELOCIMETRY WORK

Preliminary measurements of liquid vertical velocity in a hexagonal bubble column have been made during the past quarter using the laser doppler velocimeter (LDV). Efforts during the next quarter are aimed at obtaining simultaneous measurement of all three components of liquid velocity, and at also measuring the bubble velocity components nonintrusively using the LDV.

A schematic of the hexagonal cross-section bubble column is shown in Figure 3.1. The column is made of plexiglas, and is 18 cm across the flats or 21 cm across the diagonal, and can accommodate water depths up to 18 cm. For the present, preliminary experiments an air bubble injection manifold with a single, central hole of 1/16 inch diameter has been used. This results in an initial jet of air which breaks into nominal 1-2 cm diameter bubbles approximately one third of the distance up the column, which drives a relatively strong water circulation which is upwards near the central column of air bubbles, and downwards near the outer walls of the column. This configuration is being studied first because it greatly simplifies the measurement of liquid velocity because there is very little interference with the laser beams due to bubbles crossing through the beam paths away from where the laser beams cross in the measurement volume to form interference fringes. Also, the hexagonal cross-section has been selected because it eliminates the problems associated with penetrating a curved interface, while still remaining nearly cylindrical in shape. Once better alignment methods are developed, it is hoped that it will be possible to view into the flowfield normal to one face of the column with the 2-channel LDV, while simultaneously focusing on the same location with the 1-channel LDV system through a neighboring face of the column, thereby allowing 3-D velocity measurements to be made.

Preliminary vertical liquid velocity measurements have been measured versus vertical depth at the three different radial locations indicated in Figure 3.1 (2.6, 4.5, and 6.4 cm from the centerline). Air flow rate was nominally 2 SCFH. Average vertical liquid velocity (in cm/sec) versus vertical coordinate (in cm) is shown in Figure 3.2, while RMS liquid vertical velocity is shown in Figure 3.3. Measured vertical liquid velocity is positive (upwards) at 2.6 cm and 4.5 cm (near mid-radius), and essentially zero or slightly negative at 6.4 cm (approximately two-thirds the radius). Future measurements will be made at larger radii to confirm the downwards liquid velocity expected beyond 6.4 cm. Vertical liquid mean velocity is larger in the top half of the column. RMS liquid velocity is the same order of magnitude as, or larger than, the mean velocity. Fluctuations are largest at smaller radii in the top half of the column.

For these preliminary liquid velocity measurements at an air flow rate of 2 SCFH, there is essentially no re-entrainment of the air into the downward moving outer liquid flow. Thus, all LDV signals were generated by the silver-coated 5 μm diameter glass microspheres which were used to seed the liquid flow. Particles of this size essentially follow the liquid flow.

It is planned that in the future liquid vertical velocities will be measured at a greater number of radii, and that the radial liquid velocity component will be measured. Air flow rate will be increased as much as is practical, and efforts will be directed at measuring both the liquid velocity distribution and the bubble velocity distribution. Also, it is hoped that different manifolds will be used which will inject air bubbles over a larger portion of the column cross section. In as much as is practical, measurements will be obtained for bubble injection manifolds and flow rates which can be simulated using the numerical model.

4. NUMERICAL SIMULATIONS

4.1 Introduction

The modeling of circulation in a bubble column reactor has been conducted to develop understanding of the process of interaction between a dispersed phase (air bubbles) and continuous phase (water). A complete mathematical model involving the momentum exchange between the two phases has been developed, with all the terms related to the two phases are developed empirically or analytically. A typical experimental and theoretical study for a liquid circulation in a gas-liquid system has been presented by Rietema and Ottengraf (1970). The numerical simulation has been performed based on their experimental work. This section is a summary of the work done to date for the numerical simulation of circulation in a bubbly reactor.

4.2 Mathematical Model

Consider an unsteady, gas-liquid flow inside a vertically situated circular reactor which is assumed to be isothermal and non-reacting. The mathematical formulation for such two-phase flow is based on the conservation of mass and momentum principle for each phase. The gas-liquid flow is assumed to be in the bubbly flow regime which is characterized by a suspension of discrete air bubbles in a continuous liquid such as water. Let ρ_1 be the liquid macroscopic density, and ρ_2 be the gas macroscopic density such that $\rho_1=(1-\alpha)\rho_\ell$, $\rho_2=\alpha\rho_g$, where ρ_ℓ and ρ_g are the microscopic densities for liquid and gas respectively, and α is the void fraction for the gas. Let $\underline{u}_1$ be the liquid velocity vector (u_1, v_1, w_1) and $\underline{u}_2$ the gas velocity vector (u_2,v_2,w_2) in the axial x-, radial r-, and tangential, θ- directions, respectively.

Equations For Liquid Phase

The continuity equation representing the conservation of mass for the liquid phase is

$$\frac{D\rho_1}{Dt} + \rho_1(\underline{\nabla}.\underline{u}_1) = \frac{\partial\rho_1}{\partial t} + \underline{\nabla}.(\rho_1\underline{u}_1) = 0 \qquad (4.1)$$

where D( )/Dt is the substantial derivative and $\underline{\nabla}.$ is the divergence operator. The term $\underline{\nabla}.\underline{u}_1$ is zero for an incompressible flow. There are no source/sink terms in Eq.4.1 because there is no phase change due to chemical reactions or thermal changes. For numerical treatment Eq.4.1 is rewritten in conservative form as

$$\frac{\partial \rho_1}{\partial t} + \frac{1}{r}\frac{\partial}{\partial r}(\rho_1 r v_1) + \frac{1}{r}\frac{\partial}{\partial \theta}(\rho_1 w_1) + \frac{\partial}{\partial x}(\rho_1 u_1) = 0 \qquad (4.2)$$

The momentum equations for liquid phase, in vector form (see for example Celik, 1986), are

$$\rho_1 \frac{D\underline{u}_1}{Dt} = -(1-\alpha)P - \nabla\cdot\underline{\tau} + F_{12}(\underline{u}_2-\underline{u}_1) + \rho_1\underline{g} + \underline{f}_c - w_1\underline{e}_x \times \underline{u}_1/r \qquad (4.3)$$

In Eq.(4.3), the term $\nabla\cdot\underline{\tau}$ is the stress tensor, g is the acceleration of gravity, P is the mixture pressure, F_{12} is the momentum exchange function, $\underline{e}_x$ is the unit vector in x- direction, and $\underline{f}_c$ is the additional stress vector (0, $-\tau_{\theta\theta}/r$, $\tau_{r\theta}/r$) in x -, r -, and θ - directions, respectively. The components of the symmetric stress tensor $\underline{\tau}$ in cylindrical coordinates for Newtonian fluids are

$$\begin{aligned}
\tau_{xx} &= -P + 2\mu\frac{\partial u}{\partial x} - \frac{2}{3}\mu\,\nabla\cdot\underline{u} \\
\tau_{rr} &= -P + 2\mu\frac{\partial v}{\partial r} - \frac{2}{3}\mu\,\nabla\cdot\underline{u} \\
\tau_{\theta\theta} &= -P + 2\mu\left(\frac{1}{r}\frac{\partial w}{\partial \theta} + \frac{v}{r}\right) - \frac{2}{3}\mu\,\nabla\cdot\underline{u} \\
\tau_{rx} &= \tau_{xr} = \mu\left(\frac{\partial v}{\partial x} + \frac{\partial u}{\partial r}\right) \\
\tau_{r\theta} &= \tau_{\theta r} = \mu\left(\frac{\partial w}{\partial r} + \frac{1}{r}\frac{\partial v}{\partial \theta} - \frac{w}{r}\right) \\
\tau_{x\theta} &= \tau_{\theta x} = \mu\left(\frac{1}{r}\frac{\partial u}{\partial \theta} + \frac{\partial w}{\partial x}\right)
\end{aligned} \qquad (4.4)$$

The dilatation term $\nabla.\underline{u}$ will be neglected in the momentum equations, since the effect of this term is minimal even for a wide range of compressible fluid flows provided that the Mach number is less than 0.30. It should be noted, however, that $\nabla.\underline{u}$ will be kept in the equation of continuity and the resulting equations would be valid for many compressible fluid flow problems unless this term becomes very large under unusual circumstances, i.e. Mach numbers larger than 0.3.

The term $F_{12}\ (\underline{u}_2-\underline{u}_1)$ in Eq.(4.3) represents the momentum exchange for liquid-phase equations, likewise, $F_{21}(\underline{u}_2-\underline{u}_1)$ is the momentum exchange term for gas-phase equations, hence $F_{12}=-F_{21}$. If the dilatation term $\nabla.\underline{u}_1$ is neglected, the three components of Eq.4.3 in x-, r-, θ-directions, respectively, can be written in conservative form as follows

<u>x - Momentum</u>

$$\frac{\partial \rho_1 u_1}{\partial t} + \frac{\partial}{\partial x}(\rho_1 u_1 u_1) + \frac{1}{r}\frac{\partial}{\partial r}(r\rho_1 u_1 v_1) + \frac{1}{r}\frac{\partial}{\partial \theta}(\rho_1 u_1 w_1)$$

$$= \frac{\partial}{\partial x}(\tau_{xx}) + \frac{1}{r}\frac{\partial}{\partial r}(r\tau_{rx}) + \frac{1}{r}\frac{\partial}{\partial \theta}(\tau_{\theta x}) + \rho_1 g_x + F_{12}(u_2-u_1) \quad (4.5)$$

<u>r - Momentum</u>

$$\frac{\partial \rho_1 v_1}{\partial t} + \frac{\partial}{\partial x}(\rho_1 u_1 v_1) + \frac{1}{r}\frac{\partial}{\partial r}(r\rho_1 v_1 v_1) + \frac{1}{r}\frac{\partial}{\partial \theta}(\rho_1 v_1 w_1) - \rho_1\frac{w_1^2}{r}$$

$$= \frac{\partial}{\partial x}(\tau_{xr}) + \frac{1}{r}\frac{\partial}{\partial r}(r\tau_{rr}) + \frac{1}{r}\frac{\partial}{\partial \theta}(\tau_{\theta r}) - \frac{\tau_{\theta\theta}}{r} + \rho_1 g_r + F_{12}(v_2-v_1) \quad (4.6)$$

<u>θ - Momentum</u>

$$\frac{\partial \rho_1 w_1}{\partial t} + \frac{\partial}{\partial x}(\rho_1 u_1 w_1) + \frac{1}{r}\frac{\partial}{\partial r}(r\rho_1 v_1 w_1) + \frac{1}{r}\frac{\partial}{\partial \theta}(\rho_1 w_1 w_1) + \frac{\rho_1 v_1 w_1}{r}$$

$$= \frac{\partial}{\partial x}(\tau_{x\theta}) + \frac{1}{r}\frac{\partial}{\partial r}(r\tau_{\theta r}) + \frac{1}{r}\frac{\partial}{\partial \theta}(\tau_{\theta\theta}) + \frac{\tau_{r\theta}}{r} + \rho_1 g_\theta + F_{12}(w_2 - w_1) \quad (4.7)$$

For the axisymmetric, non-swirling flow case that will be investigated, Eqs.4.5-4.7 are greatly simplified. The final form of the liquid phase equations which will be solved numerically are:

Continuity

$$\frac{\partial \rho_1}{\partial t} + \frac{1}{r}\frac{\partial}{\partial r}(\rho_1 r v_1) + \frac{\partial}{\partial x}(\rho_1 u_1) = 0 \quad (4.8)$$

x - Momentum

$$\frac{\partial}{\partial t}(\rho_1 u_1) + \frac{\partial}{\partial x}(\rho_1 u_1 u_1) + \frac{1}{r}\frac{\partial}{\partial r}(r\rho_1 u_1 v_1) = -(1-\alpha)\frac{\partial P}{\partial x} + 2\frac{\partial}{\partial x}(\mu_\ell \frac{\partial u_1}{\partial x})$$

$$+ \frac{1}{r}\frac{\partial}{\partial r}(\mu_\ell \frac{\partial u_1}{\partial r}) + \frac{1}{r}\frac{\partial}{\partial r}(r\mu_\ell \frac{\partial v_1}{\partial x}) - \rho_1 g + F_{12}(u_2 - u_1) \quad (4.9)$$

r - Momentum

$$\frac{\partial}{\partial t}(\rho_1 v_1) + \frac{\partial}{\partial x}(\rho_1 u_1 v_1) + \frac{1}{r}\frac{\partial}{\partial r}(r\rho_1 v_1 v_1) = -(1-\alpha)\frac{\partial P}{\partial r} + \frac{\partial}{\partial x}(\mu_\ell \frac{\partial v_1}{\partial x})$$

$$+ \frac{2}{r}\frac{\partial}{\partial r}(r\mu_\ell \frac{\partial v_1}{\partial r}) + \frac{\partial}{\partial x}(\mu_\ell \frac{\partial u_1}{\partial r}) - \mu_\ell \frac{2v_1}{r^2} + F_{12}(v_2 - v_1) \quad (4.10)$$

Similar equations apply to the gas-phase flow. The momentum exchange function F_{12} will be prescribed empirically in the functional form

$$F_{12} = F_{12}(\alpha, Re_b) \quad (4.11)$$

where Re_b is the bubble Reynolds number defined as

$Re_b = \rho_\ell |\underline{u}_2 - \underline{u}_1| d_b / \mu_\ell$, with d_b being the bubble diameter. The explicit form of Eg.4.11 is discussed in the next subsection.

It should be noted that the way the pressure gradient terms should be handled in Egs. 4.8 - 4.10 is a controversial issue. There is considerable debate in the literature (see for example Stewart et al., 1984) whether $\nabla[(1-\alpha)P]$ or $(1-\alpha)\nabla P$ should be used in these equations. Both forms satisfy the condition that when the corresponding momentum equations for the two phases are added, the resulting pressure gradient term must be ∇P. The equal pressure model (Stewart et al. 1984) will be adopted, i.e. $P_1 = P_2 = P$; this pressure will be distributed as $(1-\alpha)P$ and αP between the liquid and gas phases, respectively. In this regard, the pressure gradient terms are being treated as part of the interfacial momentum exchange. The surface tension effects will be included in the interfacial momentum exchange function F_{12}; for different surface tension, σ, the drag force and hence the terminal velocity of a bubble are different. It should be noted, however, if we include a pressure difference $\Delta p = P_1 - P_2 = 4\sigma/d_b$ due to surface tension, this does not alter the form of the above equations. This is because the bubble diameter d_b and the surface tension, σ, are fixed for a given flow regime and hence $P_2 = P_1 + 4\sigma/d_b = P + 4\sigma/d_b$ and $\nabla P_2 = \nabla P$ again.

Once $F_{12} = F_{12}(\alpha, Re_b)$ is prescribed, Eqs.4.8 through 4.10 written for both phases constitutes a closed set of 6 differential equations for the 6 unknowns, namely α, P, u_1, v_1, u_2 and v_2. For the initial part cf the numerical simulations these equations will be reduced to 4 equations and 4 unknowns by assuming a slip velocity relation of the form

$$\underline{u}_s = \underline{u}_2 - \underline{u}_1 = f(\alpha, Re_b) \tag{4.12}$$

This explicit form of Eq.4.12 is discussed in the following sections.

Interfacial Momentum Exchange

The momentum transfer between the different phases takes place via several mechanisms, the most important of which being the viscous drag force resulting from the shear stress at the interface and the form drag due to the pressure distribution on the surface of individual bubbles. Other possible mechanisms for momentum transfer include added mass effect, magnus effect (due to rotation), pressure gradient, and shear rate effects of the surrounding fluid (see for example Hinze, 1972). For brevity these forces will not be considered in the present analysis. Instead, all these effects will be lumped into the drag function (Eq. 4.11).

In the bubbly flow regime, the total drag force can be related to that of a single bubble. Hirt (1982) used the following relation for water droplets in steam.

$$F_{12} = \frac{3}{4}\,\alpha^2(1-\alpha)\,\rho_\ell\,\frac{|\underline{u}_1 - \underline{u}_2|}{d_p}\,C_D \qquad (4.13)$$

Where d_p is the droplet particle diameter. Syamlal and O'Brien (1988) suggested the following empirical relation for dispersed solid particles in a continous liquid or gas phase

$$F_{12} = \frac{3}{4}\,\frac{\alpha^2(1-\alpha)\rho_\ell|\underline{u}_1 - \underline{u}_2|}{d_p}\,C_D^* \qquad (4.14)$$

where C_D^* is another empirical drag function given by

$$C_D^* = \frac{C_D\ (\ Re_b <= Re_b/V_r\ )}{V_r^2} \qquad (4.15)$$

In Eg. 4.15 $C_D = C_D(Re_b)$ is the drag coefficient for an isolated particle and V_r is the ratio of terminal velocity of a group of particles to that of an isolated particle. Neither of the equations 4.13 or 4.15 is strictly applicable to the bubbly flow regime. However, to a first approximation the simpler relation used by Hirt (1982) should be sufficient for our purposes, provided that C_D is replaced by an empirical relation for bubbles in water.

Such a C_D relation can be derived by curve fitting to the experimental data presented by Clift et al. (1978). For bubbles in pure systems, the following function is suggested.

$$C_D = a\, Re_b^{-b} \qquad (4.16)$$

with

$Re_b < 2$	$a = 24$	$b = 1.000$
$2 \leq Re_b < 10$	$a = 23.66$	$b = 0.981$
$10 \leq Re_b < 100$	$a = 14.9$	$b = 0.780$
$100 \leq Re_b < 1000$	$a = 6.9$	$b = 0.613$

Equations for Gas Phase

Instead of solving for the gas or momentum equations, the gas velocities will be determined from a slip velocity relation (Eq. 4.12). For small void ratios (i.e. dilute dispersed phase) the gas velocities can be calculated in the radial-direction as

$$v_s = 0 \quad \text{or} \quad v_\ell = v_g \qquad (4.18)$$

and the axial direction as

$$u_g = u_s + u_\ell$$

where the slip velocity $u_s = U_{b\infty}(1-\alpha)$ (4.19)

$U_{b\infty}$ is the terminal velocity of an isolated bubble in an infinite liquid medium. The effect of void ratio, α, on the slip velocity as given in Eq. 4.20 is suggested by Wallis(1962). $U_{b\infty}$ can be calculated by equating the drag force to the difference of the buoyancy force and the weight of the bubble. With the drag relation Eq.4.16. this force balance results in

$$U_{b\infty} = \left[\frac{4}{3a} \frac{(\rho_\ell-\rho_g)}{\rho_\ell} g \, d_b \left(\frac{\rho_\ell d_b}{\mu_\ell} \right)^b \right]^{1/(2-b)} \qquad (4.20)$$

For example with b = 1 and a = 24, i.e., Stokes range Eg. 4.20 reduces to

$$U_{b\infty} = \frac{1}{18} \frac{(\rho_\ell-\rho_g)}{\mu_\ell} g \, d_b^2 \qquad (4.21)$$

If the water (or liquid) is not pure, the degree of contamination may have significant influence on $U_{b\infty}$. For this, the empirical curves presented by Clift et al. (1978) can be used.

An alternative is to use the terminal velocity relations presented by Hewitt (1982, chapter 2) where the terminal velocity of bubbles in clean fluids is expressed as a function of Re_b and the Galileo number $G_a=g\mu_\ell/\rho_\ell\sigma^3$.

Equation for Void Fraction

The void ratio distribution, α (x,r), is not empirically specified. So the distribution function for α is determined analytically in the numerical simulation. It is assumed in the present work that α(x,r) is not varied in the vertical or axial direction, and thus it may be prescribed in the radial direction by either a parabolic function distribution

$$\alpha(r) = \alpha_c \left(1 - \frac{r^2}{R^2} \right) \tag{4.22}$$

or a cosine function distribution

$$\alpha(r) = \alpha_c (1 + Cos(\pi r/R)) \tag{4.23}$$

Here R is the tube radius, and α_c is the centerline value of α which will be related to the total gas hold-up α_T and hence to the air flow rate Q_a. Based on the experiments situation, a smoothly varying function of the form

$$\alpha(r)=0.5\ \alpha_c(1+Cos(\pi r/R_s)) \qquad r \leqslant R_s$$

with (4.24)

$$\alpha(r)=0. \qquad r > R_s$$

was selected for the simulations. Here R_s is the radius of the bubble street measured from the center of the column reactor. The center line value, α_c, was determined from conservation of mass for the gas phase, i.e.,

$$Q_a = \int_0^R 2\pi\ \alpha(r)\ u_g(x,r)\ r\ dr \tag{4.25}$$

4.3 Experimental Situation

A laminar liquid circulation and bubble street formation were investigated in a Quickfit glass column (Rietema and Ottengraf, 1970). The geometric configuration for the glass column is shown in Fig.4.1. The experimental conditions for the case simulated numerically are liquid density ρ_ℓ =1153 kg/m³, liquid viscosity μ_ℓ=350 cp (0.35 kg/m-s), air flow rate Q_a=11.4cm^3/s, gas hold-up ε_g=74 cm^3, bubble diameter d_b=0.54 cm and bubble street diameter D_s=10.0 cm. The liquid used in the experiments was a glycerol water solution. The glass column had a diameter of 22 cm and a height of 122 cm. Initially the column was filled with the liquid solution up to a depth of 80 cm. If the gas hold-up of 74 cm^3 is added to the liquid volume, the total mixture volume requires a column height of 80.195 cm. This value was used in the simulations. Air bubbles were formed by means of injection needles. According to experiments, the vertical baffles were placed along the wall, thus a reasonably symmetrical street could be created. The effect of baffles is not considered at present study.

4.4 Computational Details

The mathematical model has been incorporated in a readily available computer code, TEACH (Gosman and Ideriah, 1976; Durst and Loy, 1984). The code is based on the finite volume approach (see for example Patankar, 1980) and it is suitable for numerical solution of incompressible, steady, single phase flow problems. All the necessary modifications have been made to include the second phase in the calculation procedure. At present the computer program can be used to calculate both components of the liquid velocity distribution in an axisymmetric configuration, as well as the pressure distribution for any given void fraction radial distribution.

The calculation domain was fixed at 80.2 cm in the axial and 11 cm in the radial directions; due to symmetry, only half of the column needs to be considered in the simulations. The uniform grid distribution is used in axial and radial directions with Δx=0.04m and Δr=0.01m for testing of the numerical procedure. An adapted grid distribution should be used for more accurate calculation, since the computer code is able to accommodate a variable step size.

Initially, the liquid velocity field is not known. The gas velocity, u_g, was calculated from

$$u_g = u_\ell + u_s$$

where u_ℓ is liquid velocity and u_s is the slip velocity between the two phases. To start the calculations the liquid velocity was set equal to zero and the slip velocity was calculated from $u_s = U_{b\infty}(1-\alpha)$, $U_{b\infty}$ is prescribed as a function of the bubble Reynolds number, $U_{b\infty}$=5.23 cm/s calculated by Eq.4.21. For the conditions summarized above, an α_c value of 0.0985 was calculated with u_ℓ=0. Once α_c is determined, $\alpha(r)$ can be calculated by Eq.4.24 and the resulting α distribution at x=0 is depicted in Fig. 4.2. Then the computer program continues to solve the liquid momentum equations for u_ℓ and v_ℓ, and solve liquid continuity equations for pressure. The liquid velocities are corrected after the pressure calculation. The result indicates that the solution converges after about 300 iteration steps. A relaxation factor of 0.7 was used for the $\alpha(r)$ calculation in the first 100 iteration steps.

4.5 Results and Discussion

Rietema and Ottengraf (1970) have presented the velocity profiles from their experimental work, see Fig.4.3. The velocity profiles were measured half way up the column height (at x=40cm) by following very small dispersed air bubbles, which move at the local liquid velocity. The operating conditions used for the numerical calculations are the same as the experiments: the dimensionless air flow rate

$q_a=(8\mu/\pi\rho_\ell gD^4)Q_a=$ 0.3874×10^{-6}, where D is column diameter, and $Q_a=11.4cm^3/s$, air flow rate; Diameter ratio $\delta=D_s/D=0.454$; and dimensionless slip velocity $(\mu_\ell/\rho_\ell gD^2)u_s=0.428\times10^{-4}$. The bubble Reynolds number Re_b is about 0.9 according to the calculation, so the Stokes equation can be used for such a laminar flow. The void fraction $\alpha(x,r)$ is calculated at each grid point of the cross section along the axial direction. Fig. 4.2 shows the result of the void fraction distributions. The curve at x=0 is the void fraction distribution imposed at the inlet of the column. The void fraction distribution changes gradually, but after half way up the column (x=40cm), the distribution seems unlikely to change any more. The liquid velocity profile from the experiments is shown in Fig.4.3, and the liquid velocity profiles from the calculation are shown in Fig. 4.4. By comparing the results at x=40cm, the magnitude of liquid velocity in the calculation at the reactor center line is about twice that in the experiment, however the shape of velocity profile and magnitude of liquid velocity near the wall are close to that from the experiment.

The calculated stream function contours for the liquid phase are plotted in Fig.4.5. This stream function is defined as

$$\psi = 2\pi \int \alpha \, \rho_\ell \, u_\ell \, r \, dr \tag{4.26}$$

The result has been improved and there is no flow separation predicted. It is seen that the usual counter clockwise recirculation pattern is predicted correctly for the liquid phase.

4.6 Conclusions

Progress has been made in the numerical simulation for the bubbly flow in a vertically situated circular reactor.

The mathematical model for liquid-gas two-phase flow has been developed. A slip velocity relation is prescribed empirically from which the gas phase velocity is calculated. The results show that the simplified model for the gas phase is workable for the general prediction.

The void fraction $\alpha(r)$ is described by a smoothly varying cosine function. The void fraction distribution function is a key point in the connection of the liquid and gas phases calculations. The results from the liquid velocity profile has indicated that the function for the $\alpha(r)$ distribution is in good agreement with the experiments. For future investigations, the $\alpha(r)$ function will be tested and matched more realistically to the experimental situation, such as including the baffles effect.

The numerical results show the correct patterns and shapes for the stream lines and liquid velocity profiles in comparison of the experimental results, but there is the discrepancy in the magnitude of the liquid velocity at the centerline of the column.

REFERENCES

-Celik, I., "Computational Fluid Dynamics Assessment", Quarterly Technical Rept., Mech. & ero. Engr. Dept., Oct. 1985-Jan. 1986, West Virginia Univ., 1986.

-Clift, R., J.R. Grace and M.E. Weber, Bubbles, Drops, and Particles, Academic Press, 1978.

-Durst, F., and Loy, T. (1984) "TEACH: Ein Berechnungsverfahren fuer zweidimensionale laminare and turbulente Stroemungen," Report, Institut fuer Hyromechanik, Universtaet Karlsruhe, Karlsruhe, F.R.Germany.

-Gosman, A.D. and F.J.K. Ideriah (1976), "Teach-2E: A General Computer Program for Two-Dimensional, Turbulent Recirculating Flows," Report without number, Dept. of Mech. Engrg, Imperial College, London.

-Hewitt, G.F., "Liquid-gas System: Void Fraction", in Handbook of Multiphase Systems, Hetsroni, G. ed., Hemisphere Publishing Corporation, McGraw-Hill Publishing Company, 1982.

-Hinze, J.O., "Turbulent Fluid and Particle Interaction", Progress in Heat and Mass Transfer, 6, Oxford, 1972, pp.433-452.

-Hirt, C.W., "Numerical Fluid Dynamics", A short course, Flowscience Inc., Los Alamos, New Mexico, 1982.

-Patankar, S.V., (1980) Numerical Heat Transfer and Fluid Flow, Hemisphere Publ. Corp., New York.

-Rietema, K. and Ottengraf, S.P.P., (1970) "Laminar Liquid Circulation and Bubble Street Formation in a Gas-Liquid System," Trans. Inst. Chem. Engrs., Vol.48, pp.T54-T62.

-Stewart, H.B. and B. Wendroft (1984), "Two-Phase Flow: Models and Methods", J.Comput. Phys. 56, pp.363-409.

-Syamlal, M. and O'Brien, T.J., "Simulation of Granular Layer Inversion in Liquid Fluidized Beds," Int. J. Multiphase Flow, 14, No.4, 1988, pp.473-481.

-Wallis, G.B., in Rottenburg, P.A.(Ed.), "Interaction Between Fluids and Particles", 1962, p.9, (London, The Institution of Chemical Engineers).

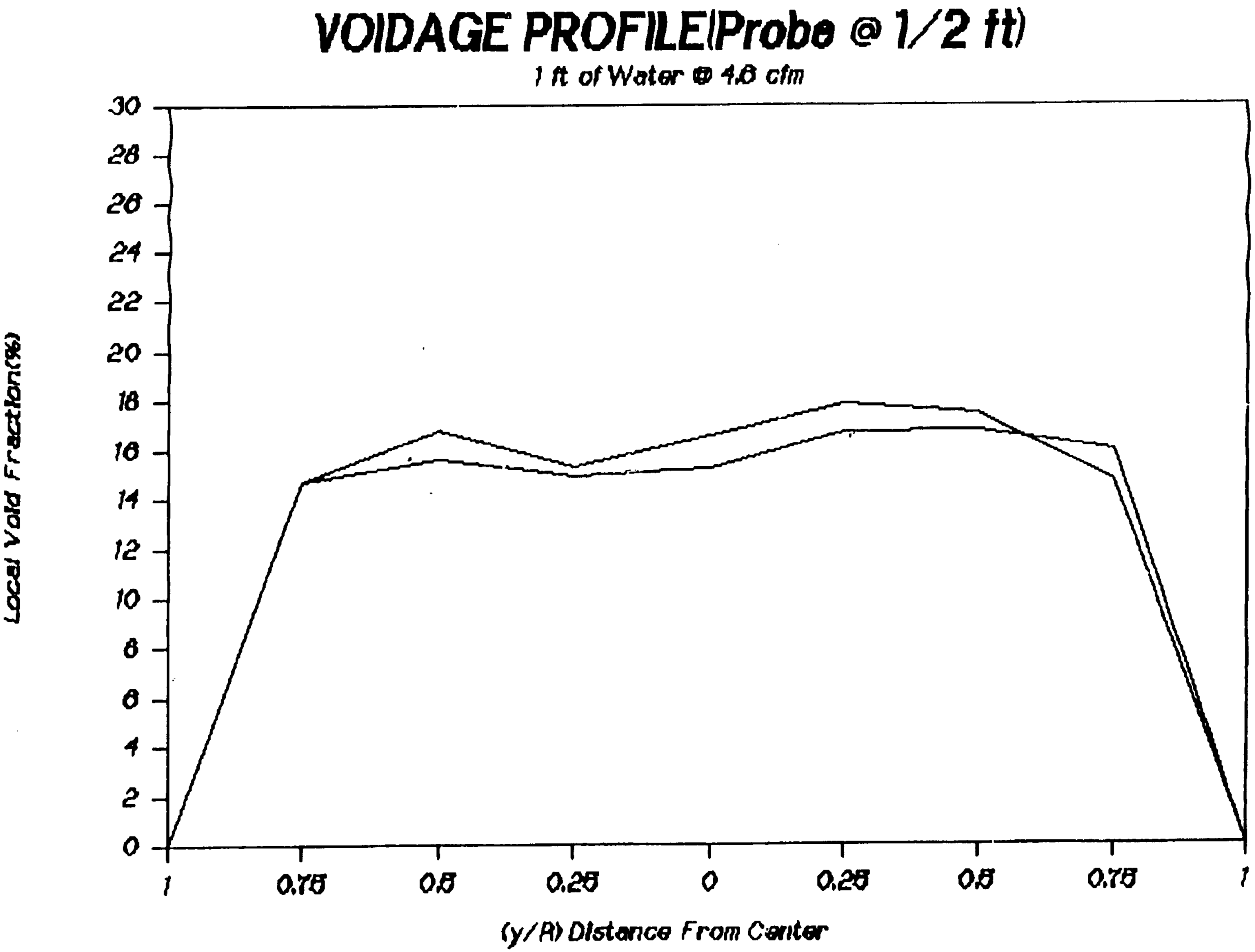

Figure 2.1 Voidage Profile at 6" (1 ft. of water and Q_a = 4.6 CFM)

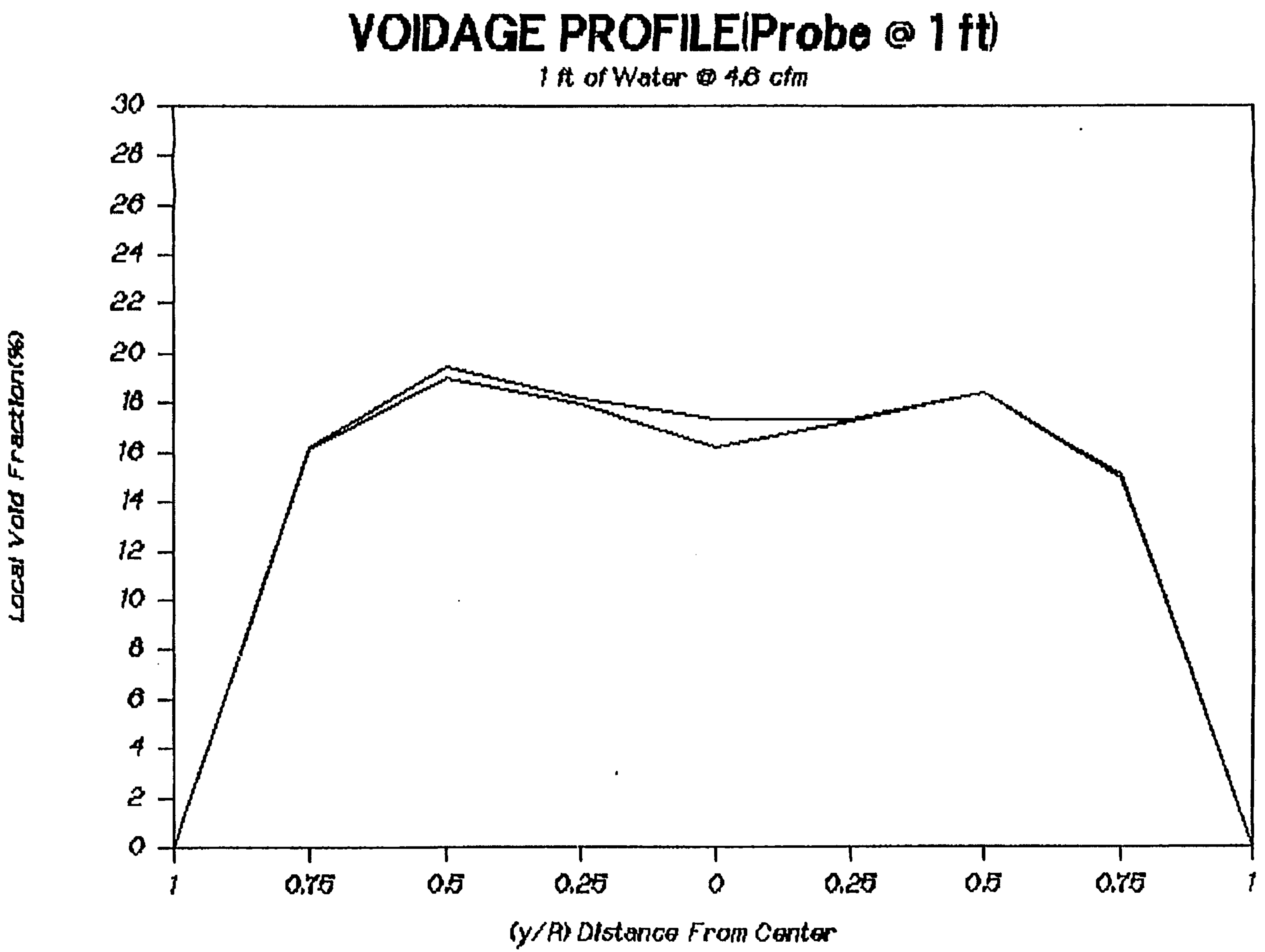

Figure 2.2 Voidage Profile at 12" (1 ft. of water and Q_g = 4.6 CFM)

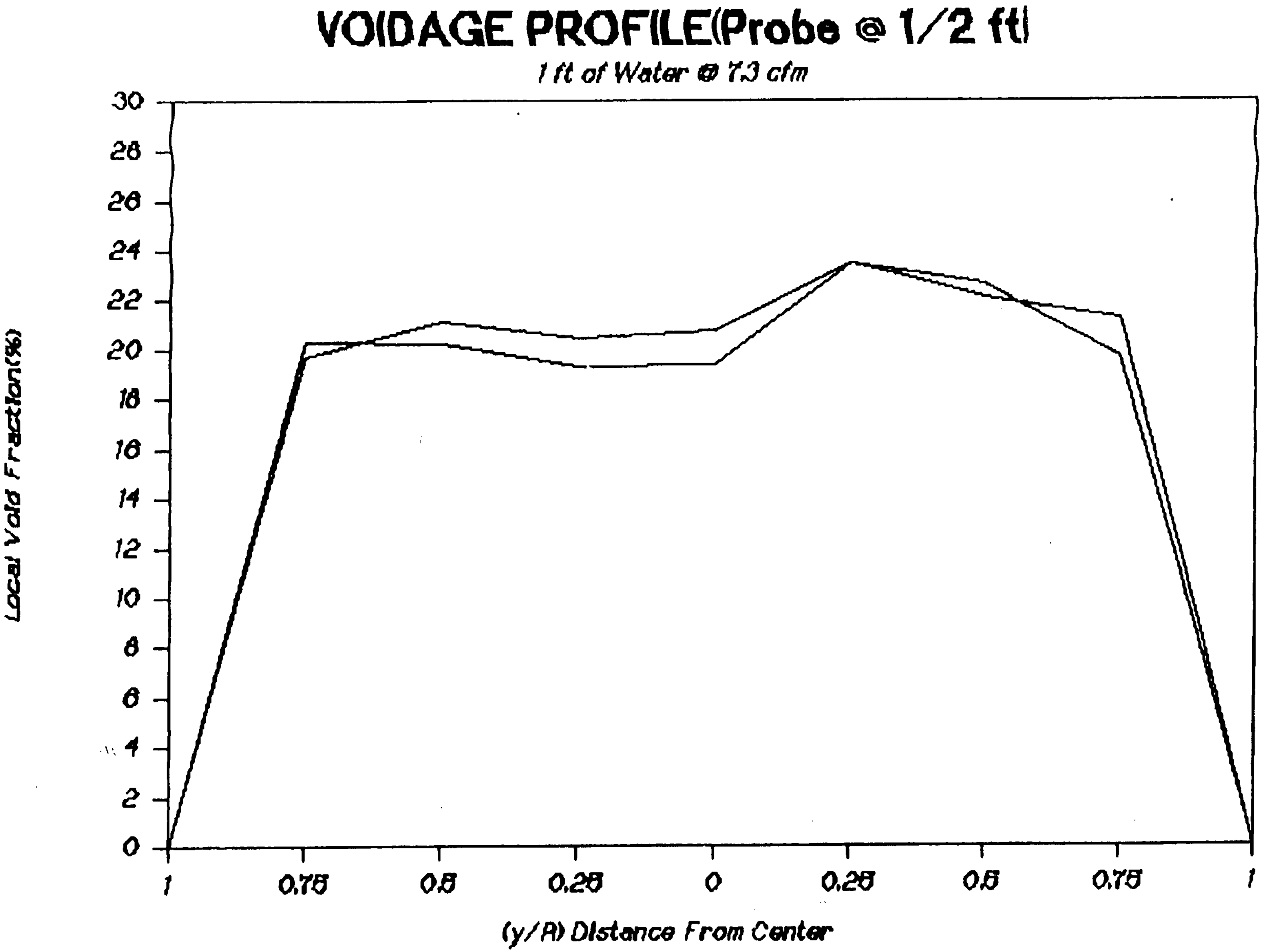

Figure [illegible] Voidage Profile at 6" (1 ft. of water and Q = 7.3 CFM)

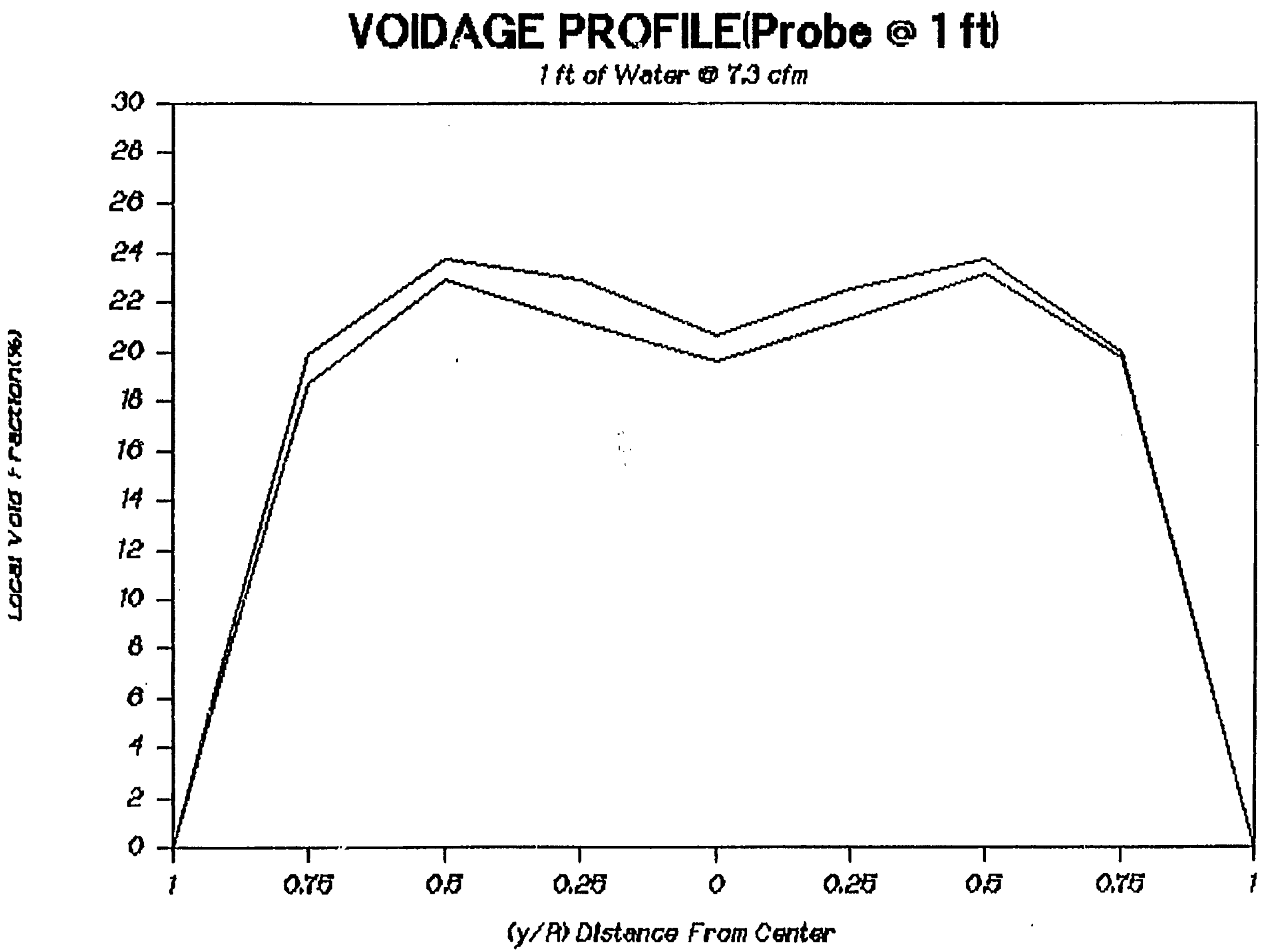

Figure 2.4 Voidage Profile at 12" (1 ft. of water and Q_g = 7.3 CFM)

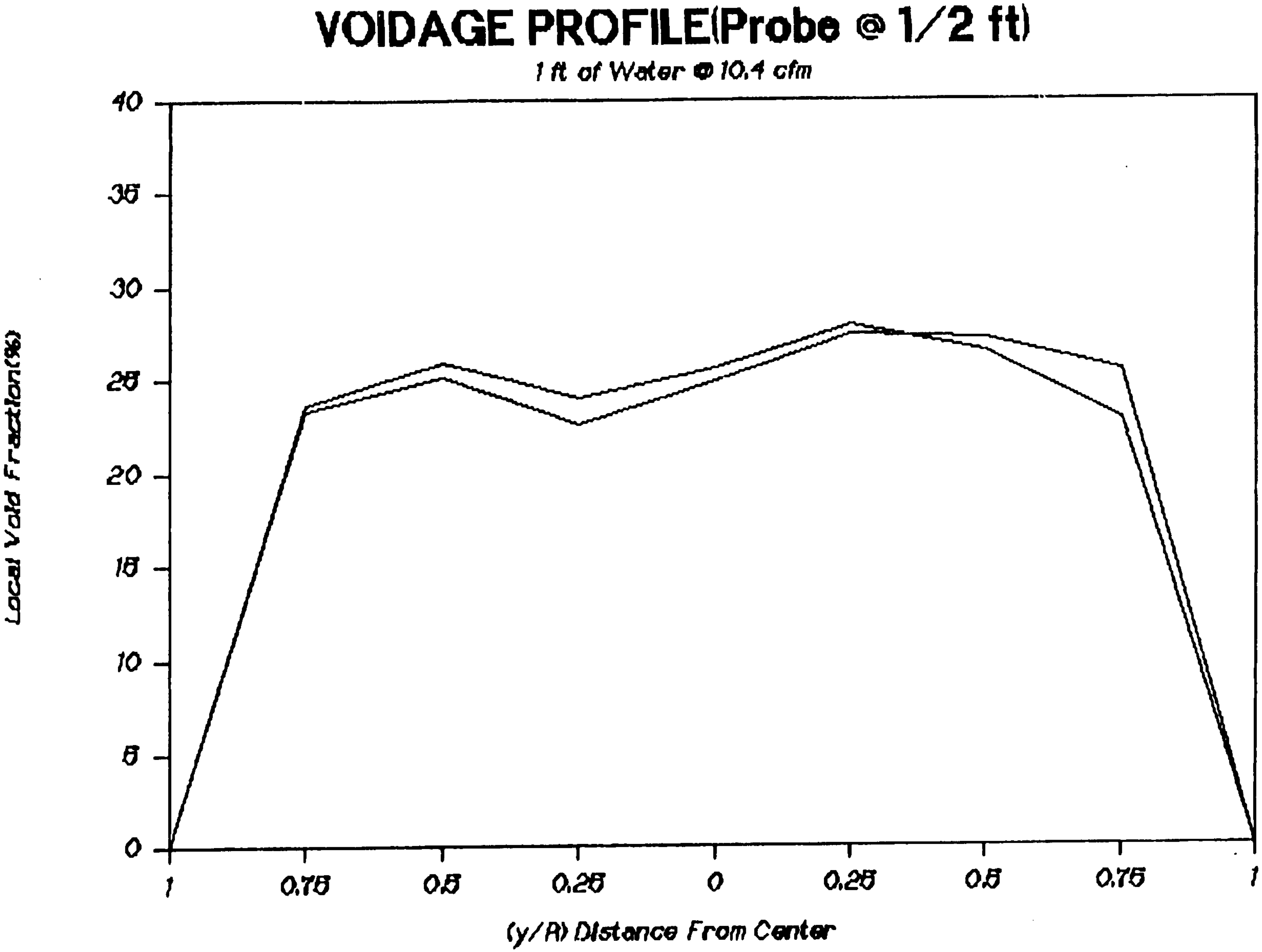

Figure 2.5 Voidage Profile at 6" (1 ft. of water and Q_g = 10.4 CFM)

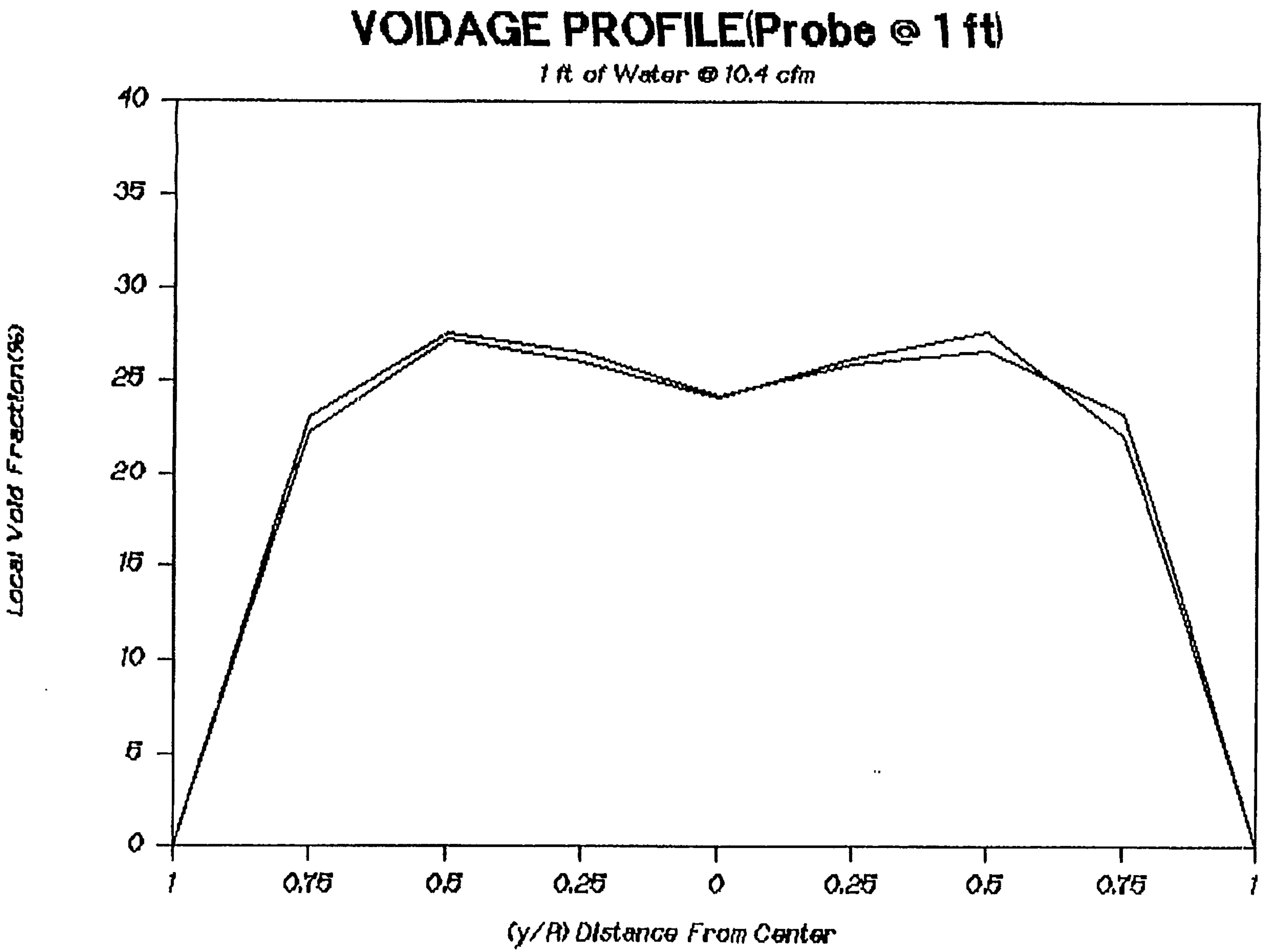

Figure 2.6 Voidage Profile at 12" (1 ft. of water and Q_g = 10.4 CFM)

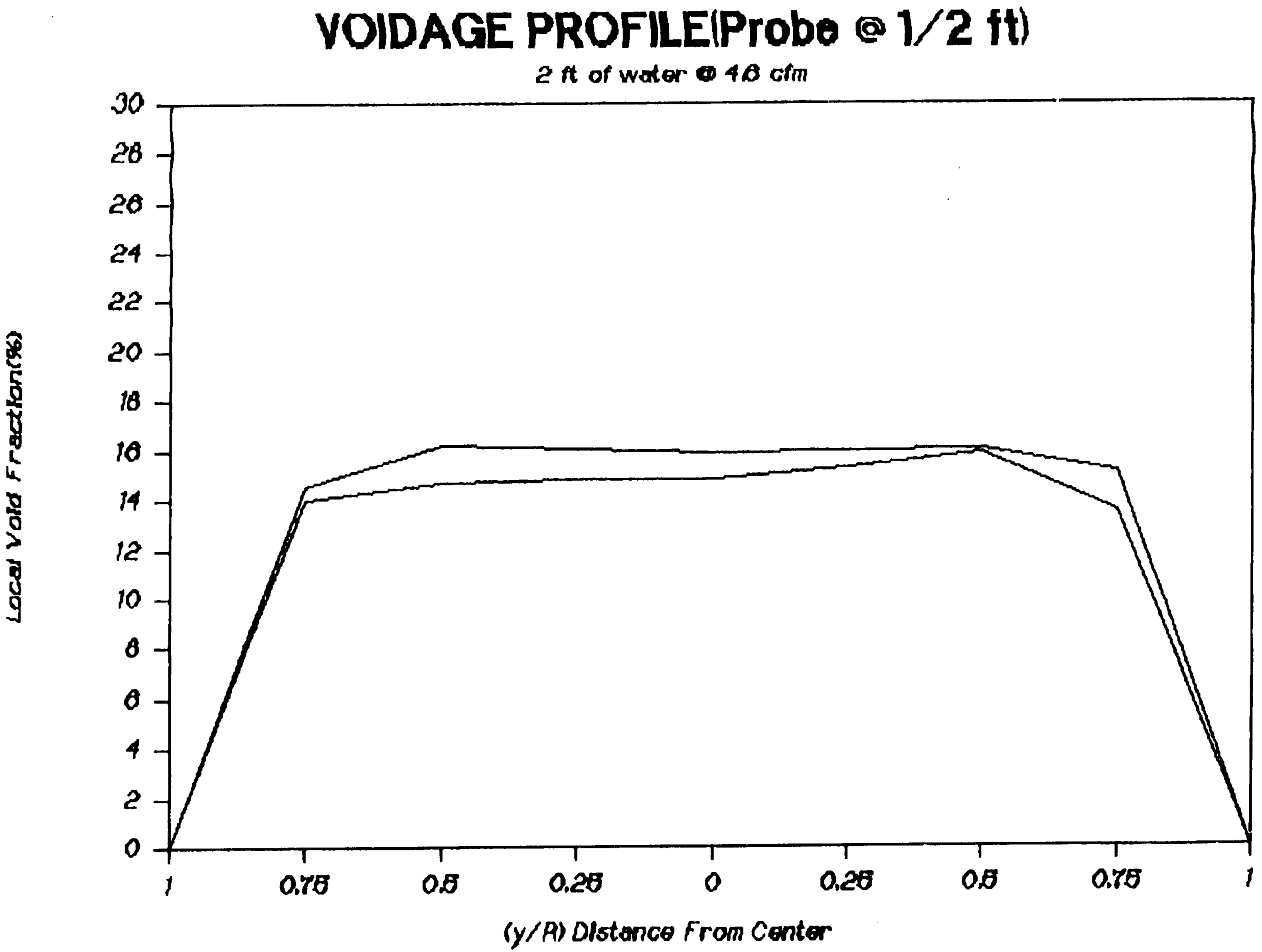

Figure 2.7 Voidage Profile at 6" (2 ft. of water and Q_g = 4.6 CFM)

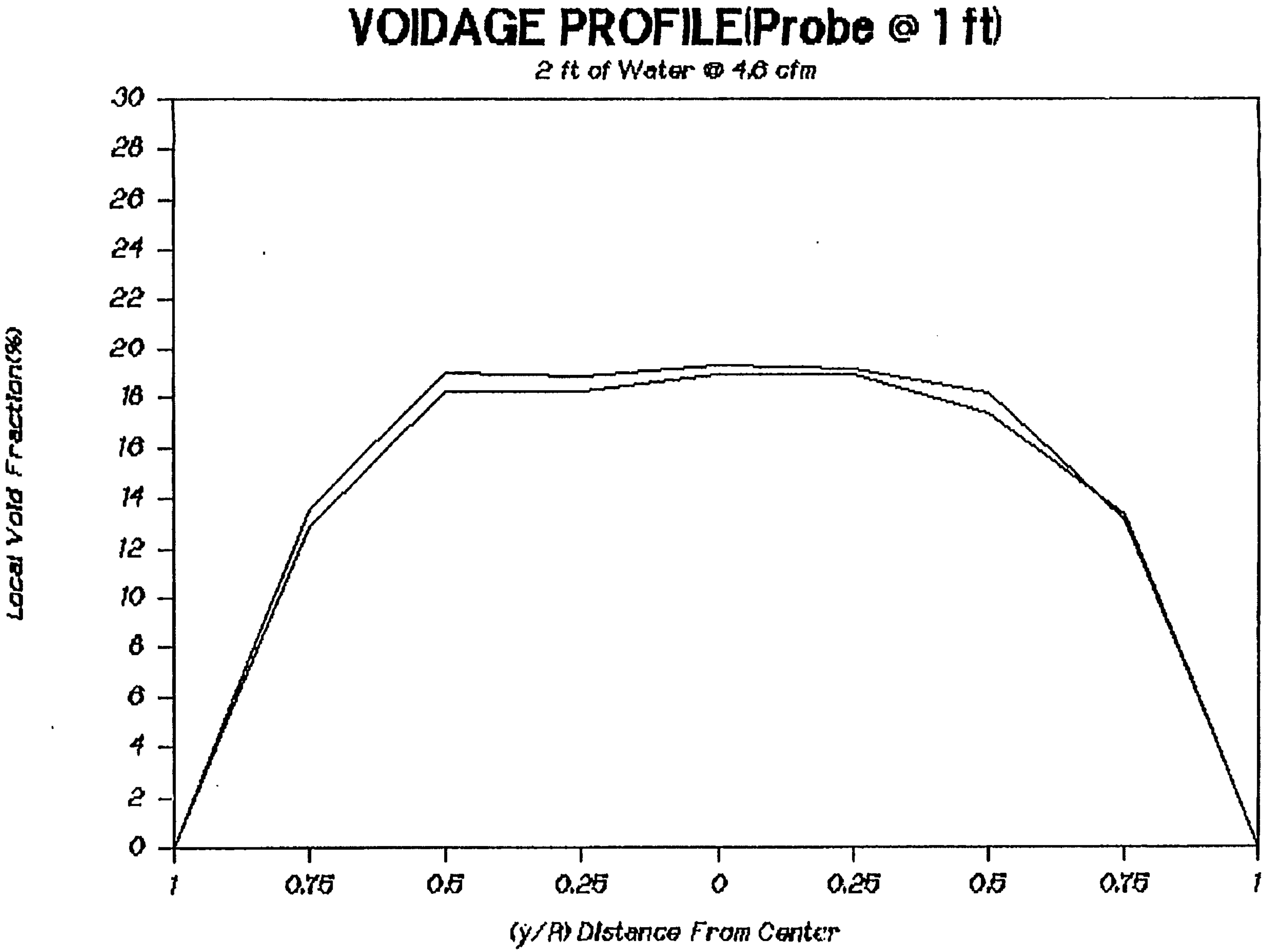

Figure 2.8 Voidage Profile at 12" (2 ft. of water and Q_g = 4.6 CFM)

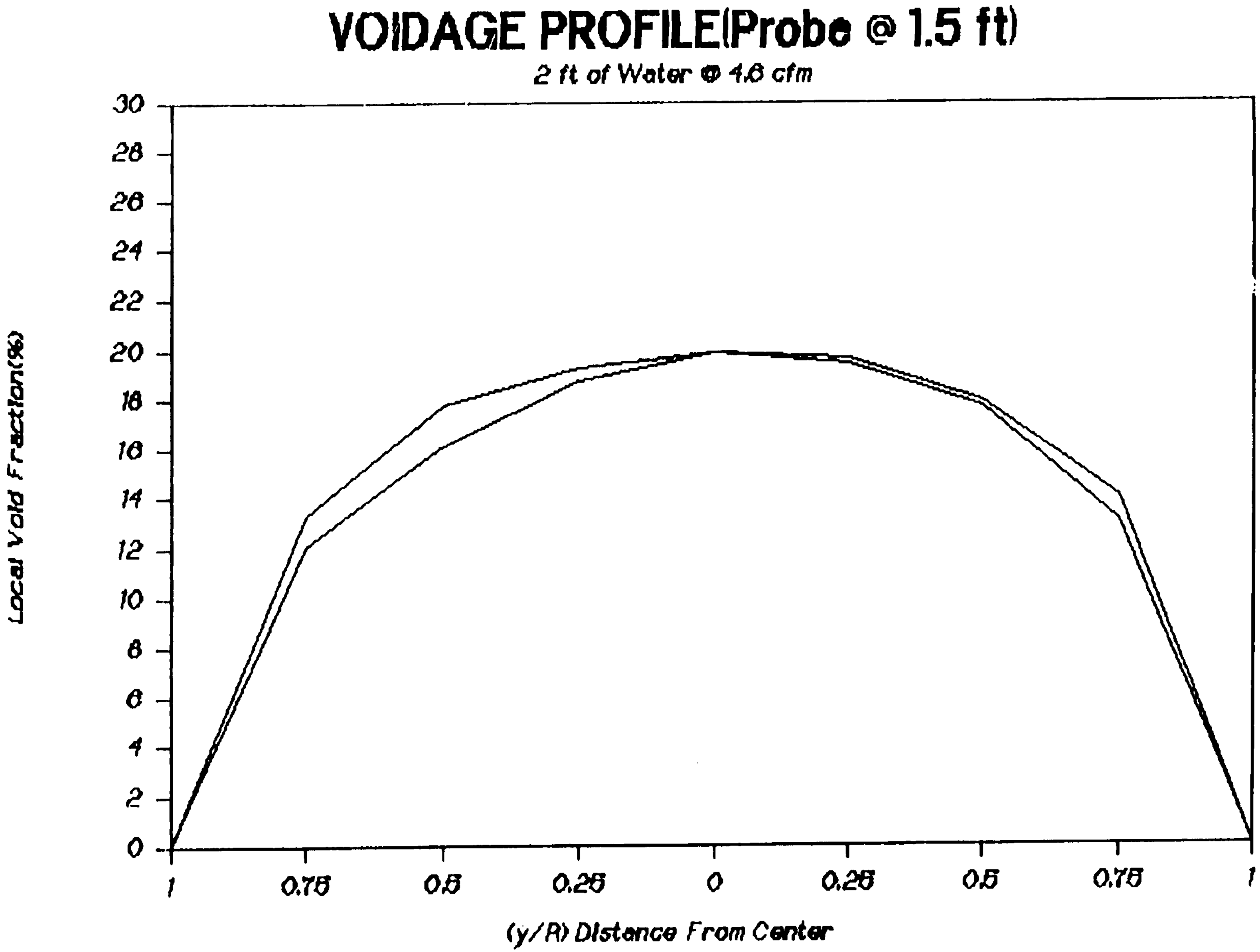

Figure 2.9 Voidage Profile at 18" (2 ft. of water and Q_g = 4.6 CFM)

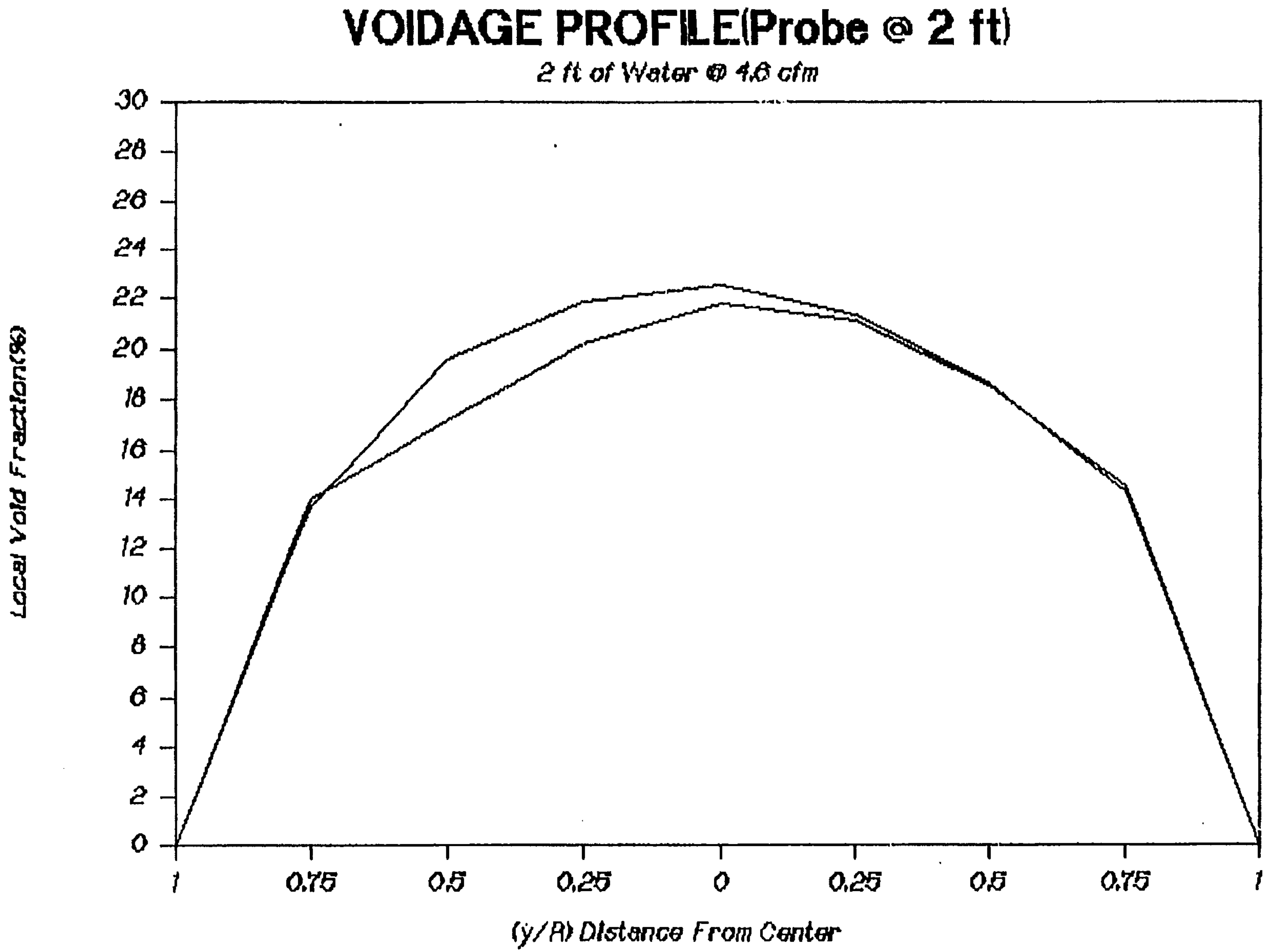

Figure 2.10 Voidage Profile at 24" (2 ft. of water and Q_g = 4.6 CFM)

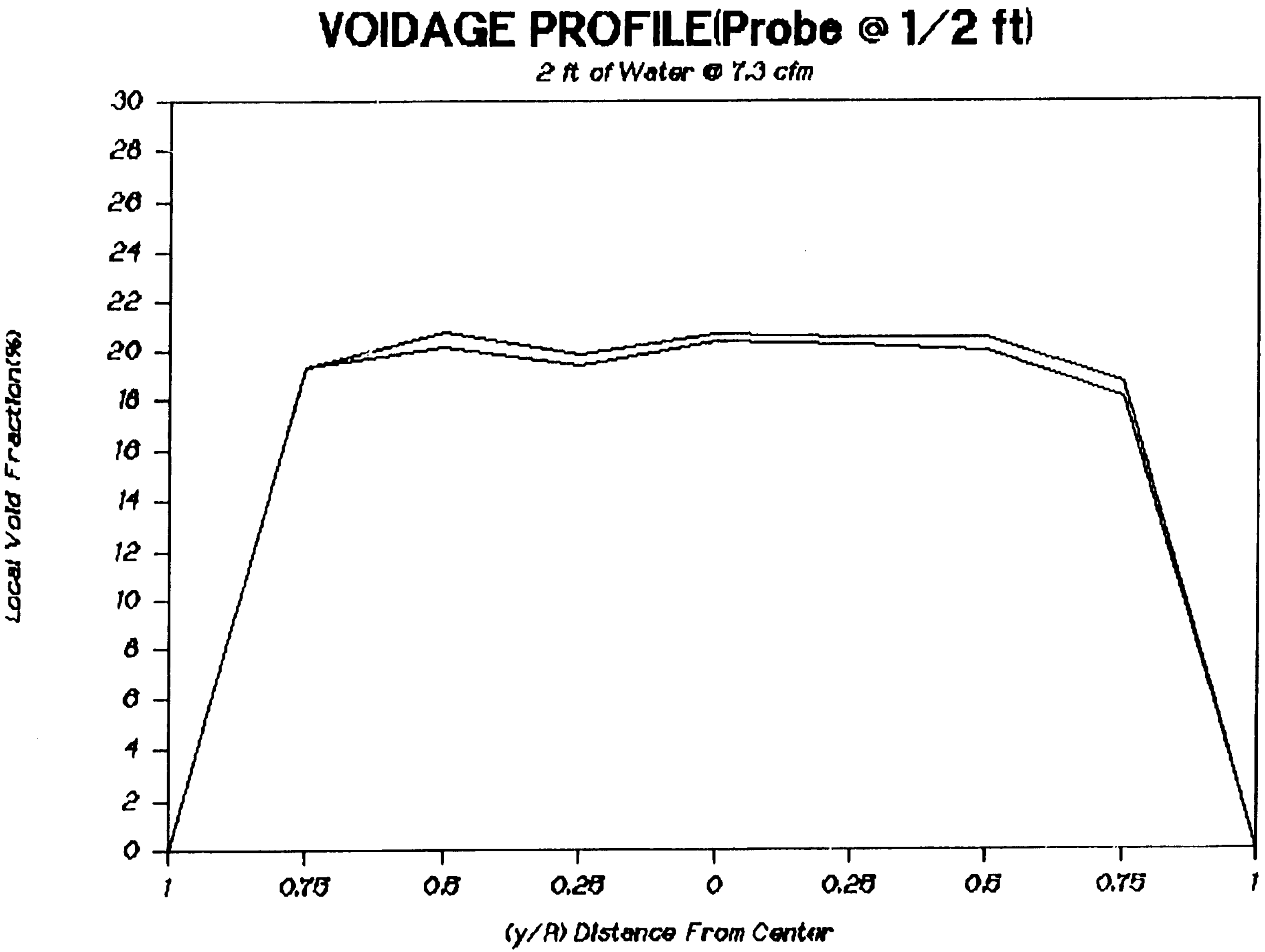

Figure 2.11 Voidage Profile at 6" (2 ft. of water and Q_g = 7.3 CFM)

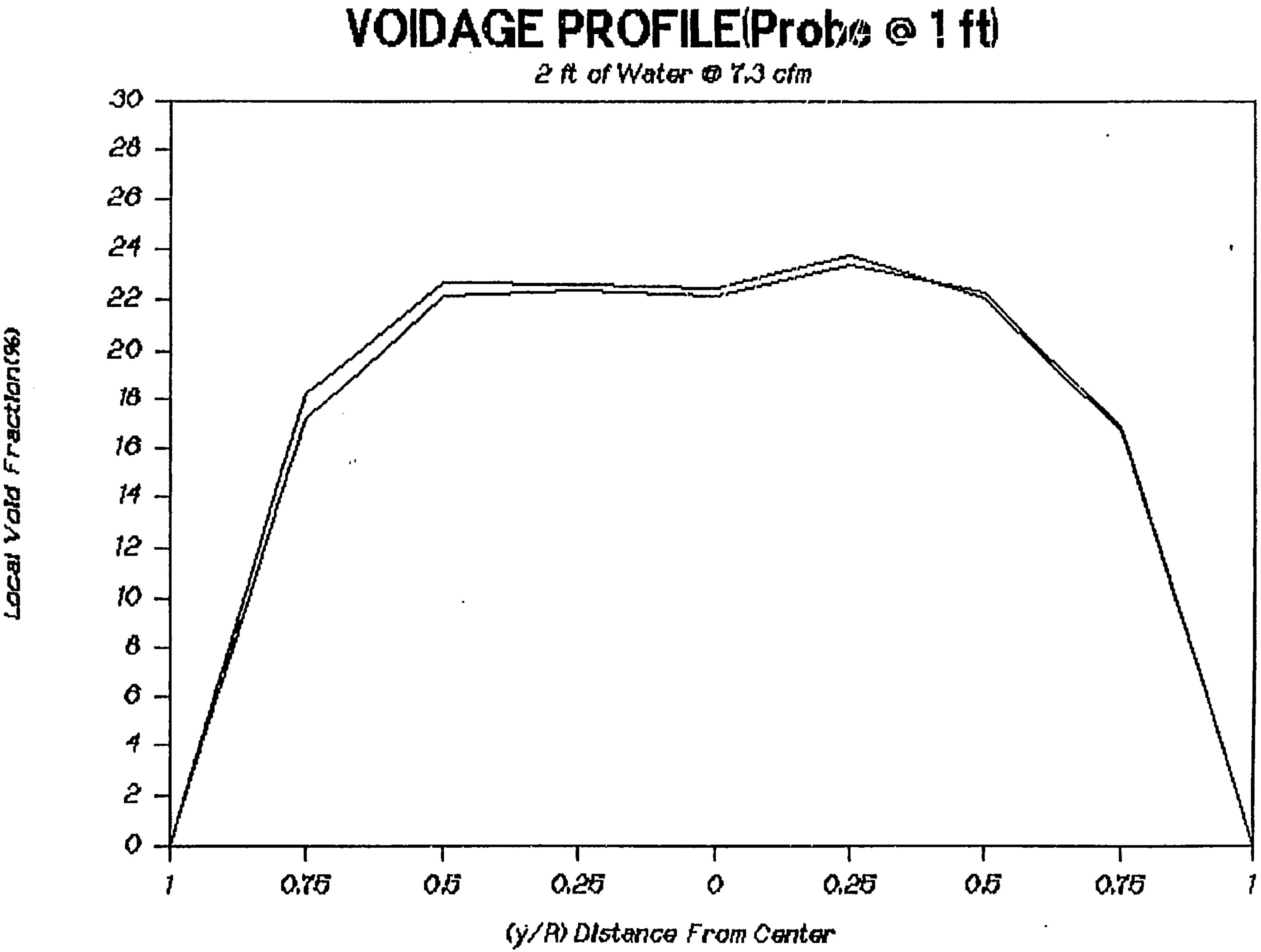

Figure 2.12 Voidage Profile at 12" (2 ft. of water and Q_g = 7.3 CFM)

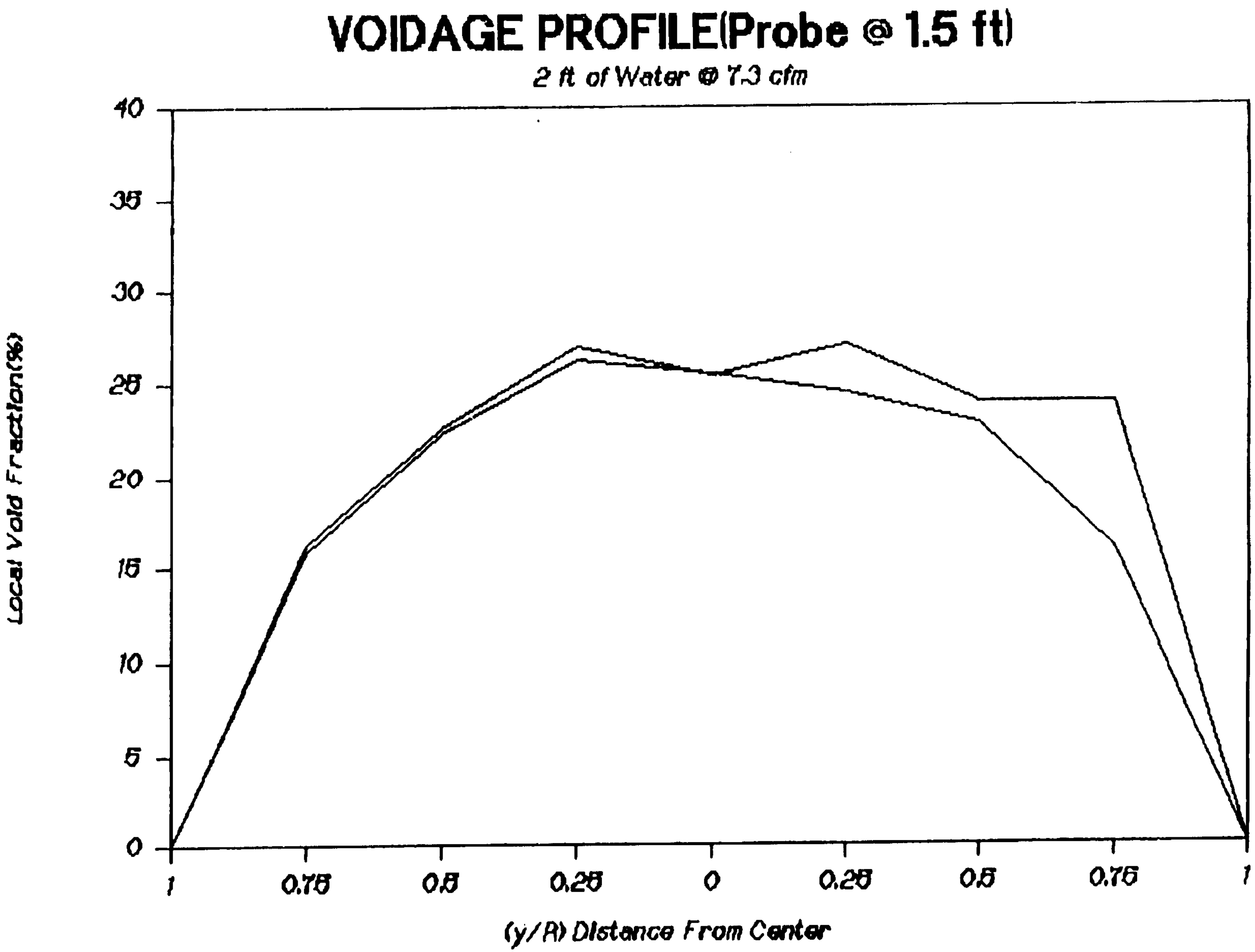

Figure 2.13 Voidage Profile at 18" (2 ft. of water and Q_g = 7.3 CFM)

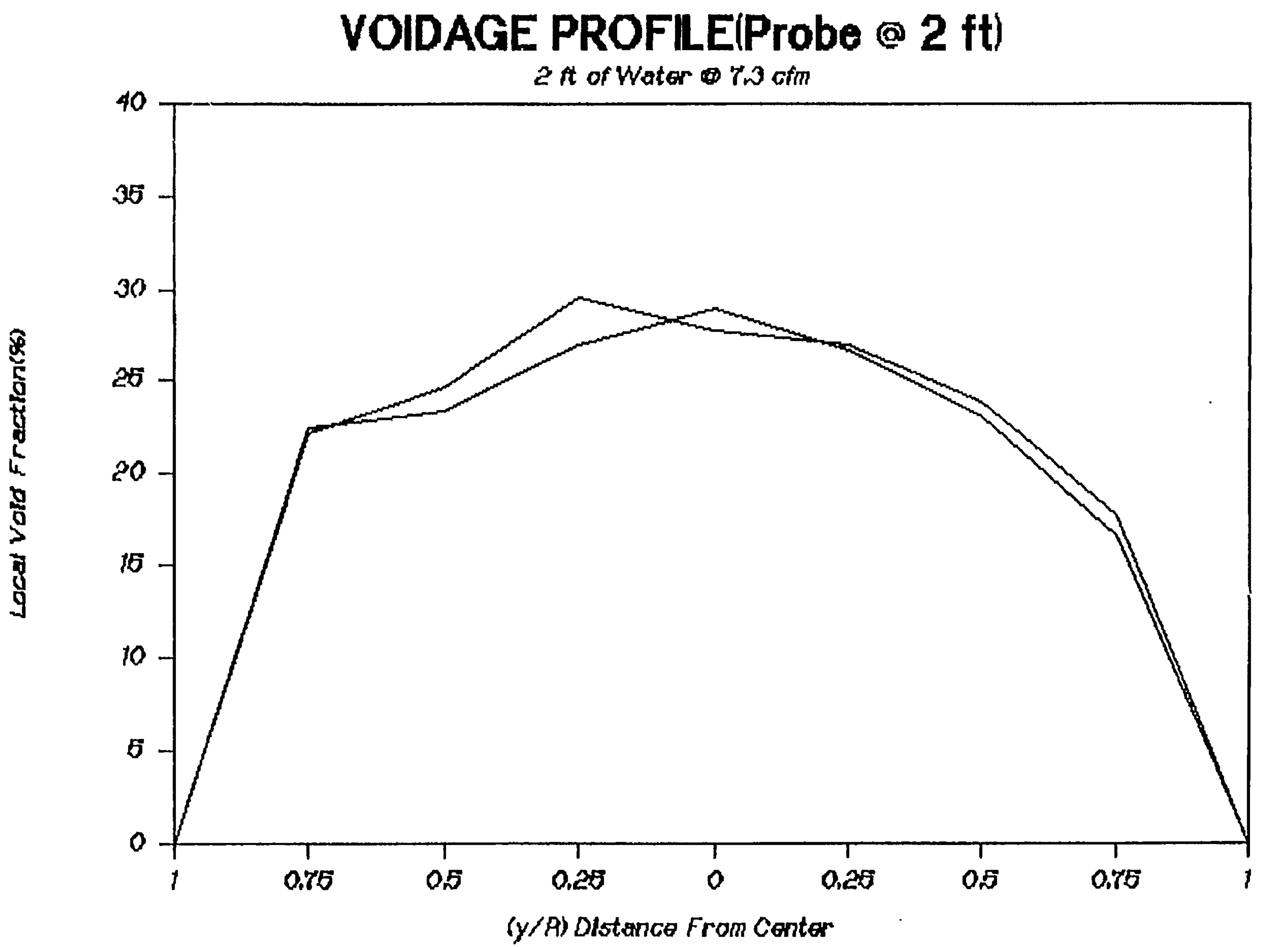

Figure 2.14 Voidage Profile at 24" (2 ft. of water and Q_g = 7.3 CFM)

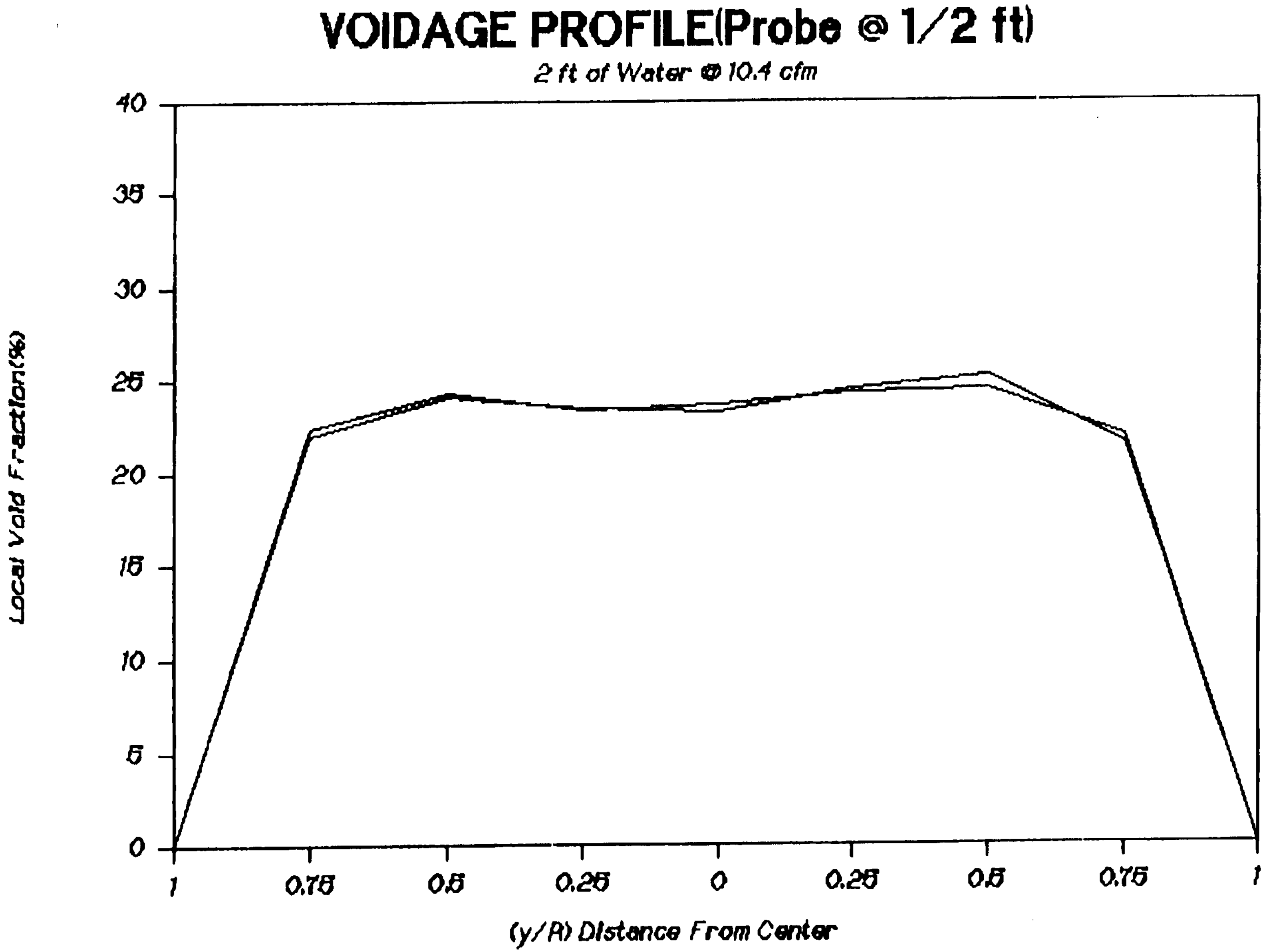

Figure 2.15 Voidage Profile at 6" (2 ft. of water and Q_g = 10.4 CFM)

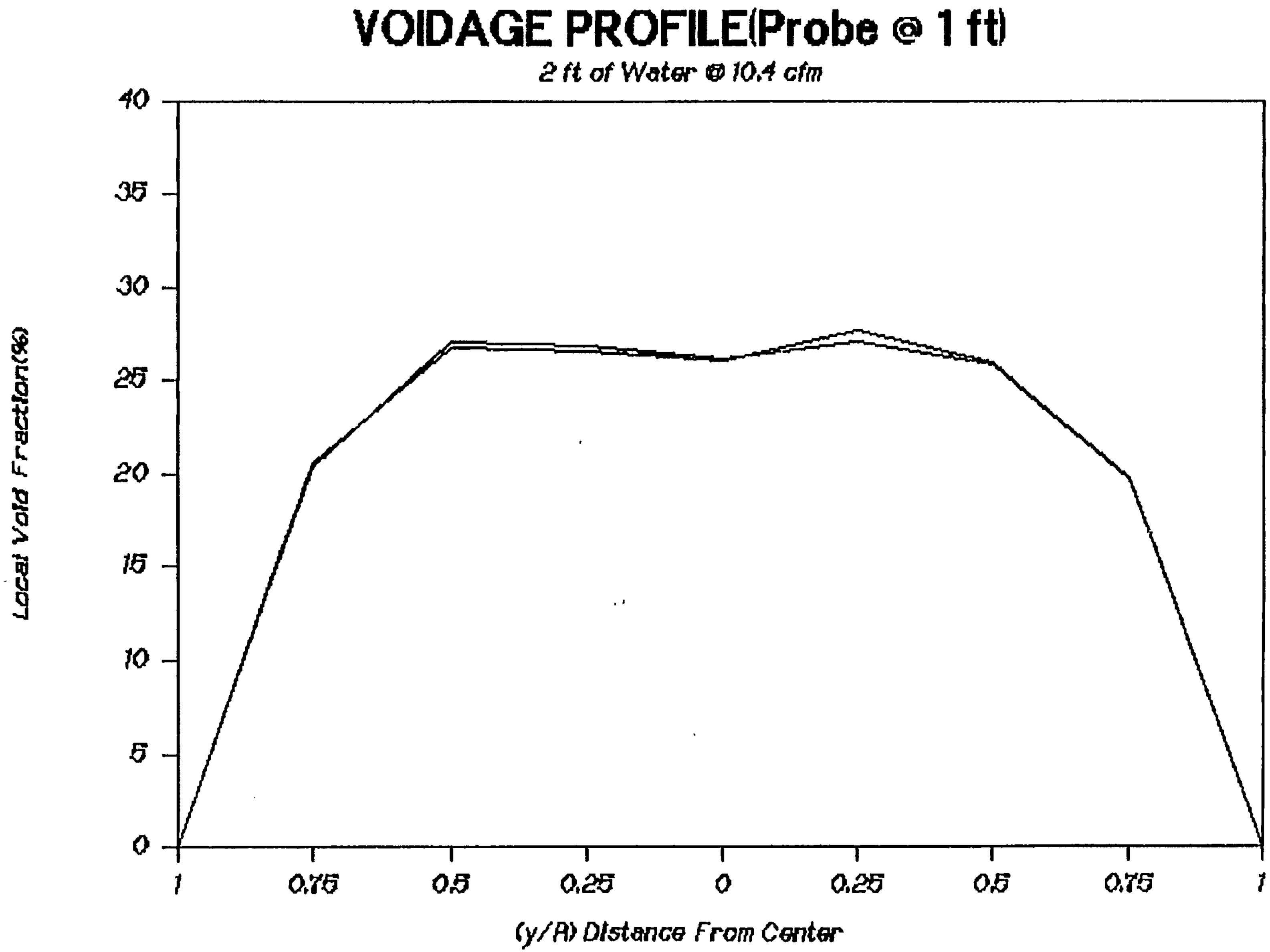

Figure 2.16 Voidage Profile at 12" (2 ft. of water and Q_g = 10.4 CFM)

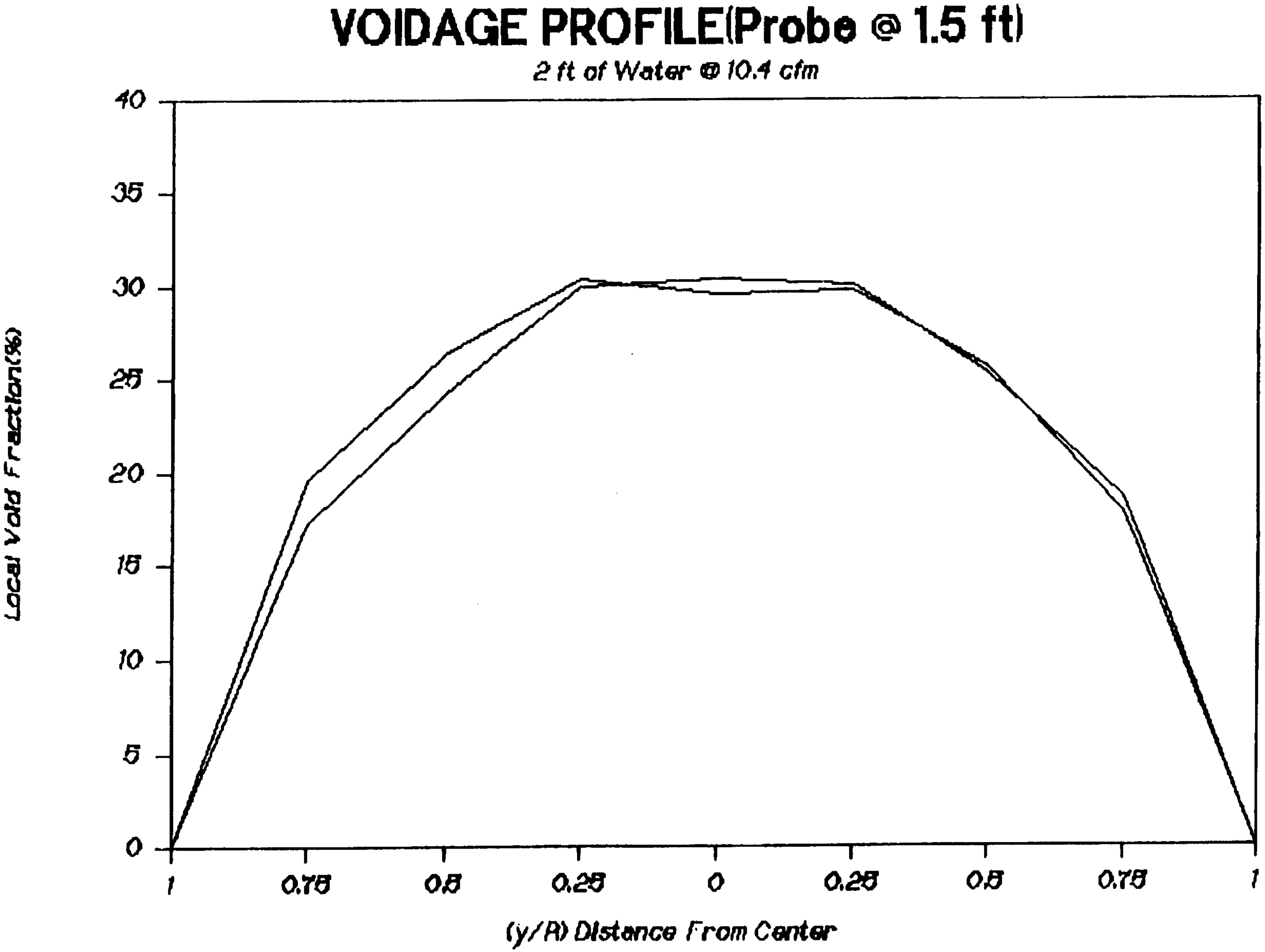

Figure 2.17 Voidage Profile at 18" (2 ft. of water and Q_g = 10.4 CFM)

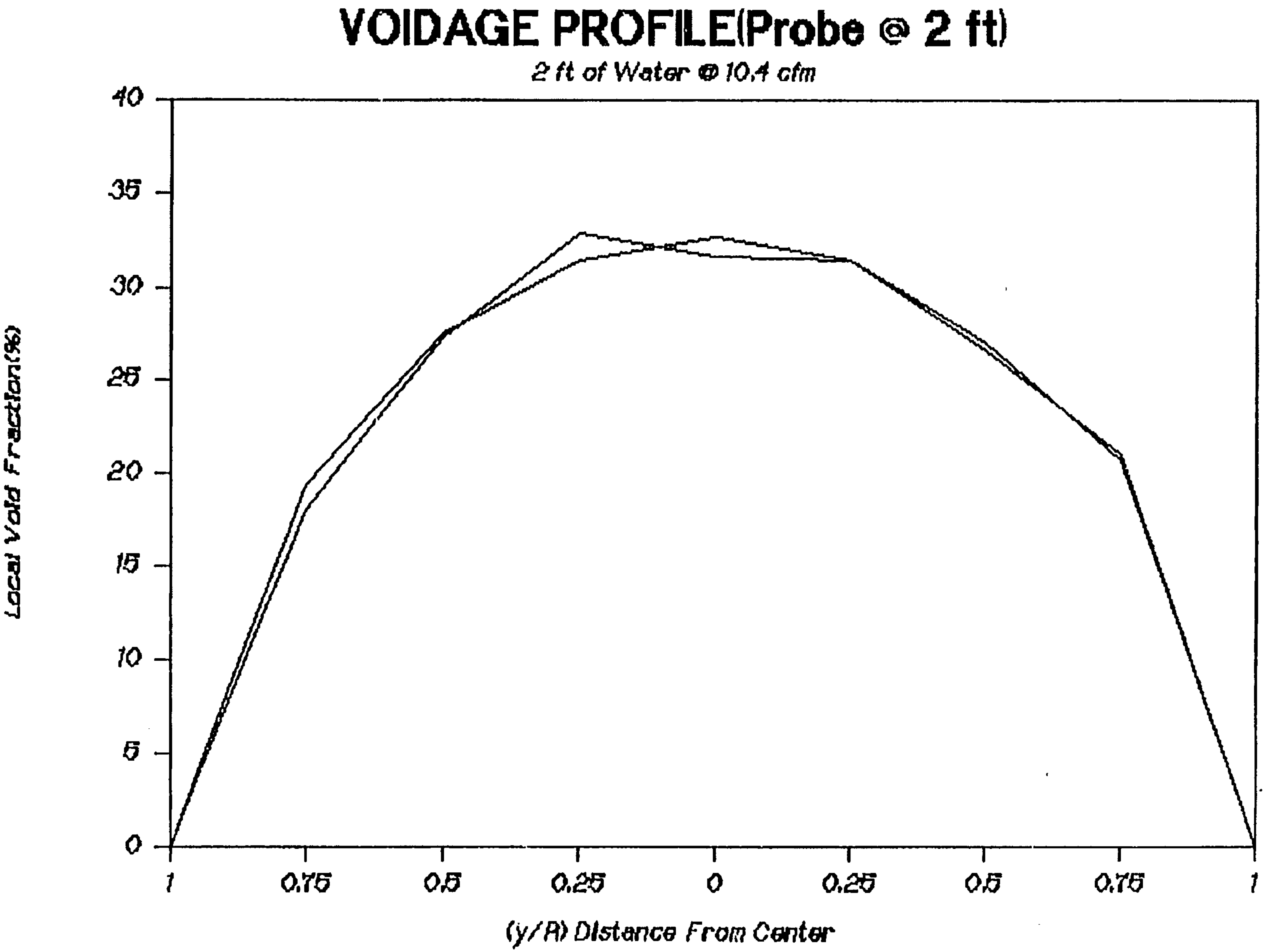

Figure 2.18 Voidage Profile at 24" (2 ft. of water and Q_g = 10.4 CFM)

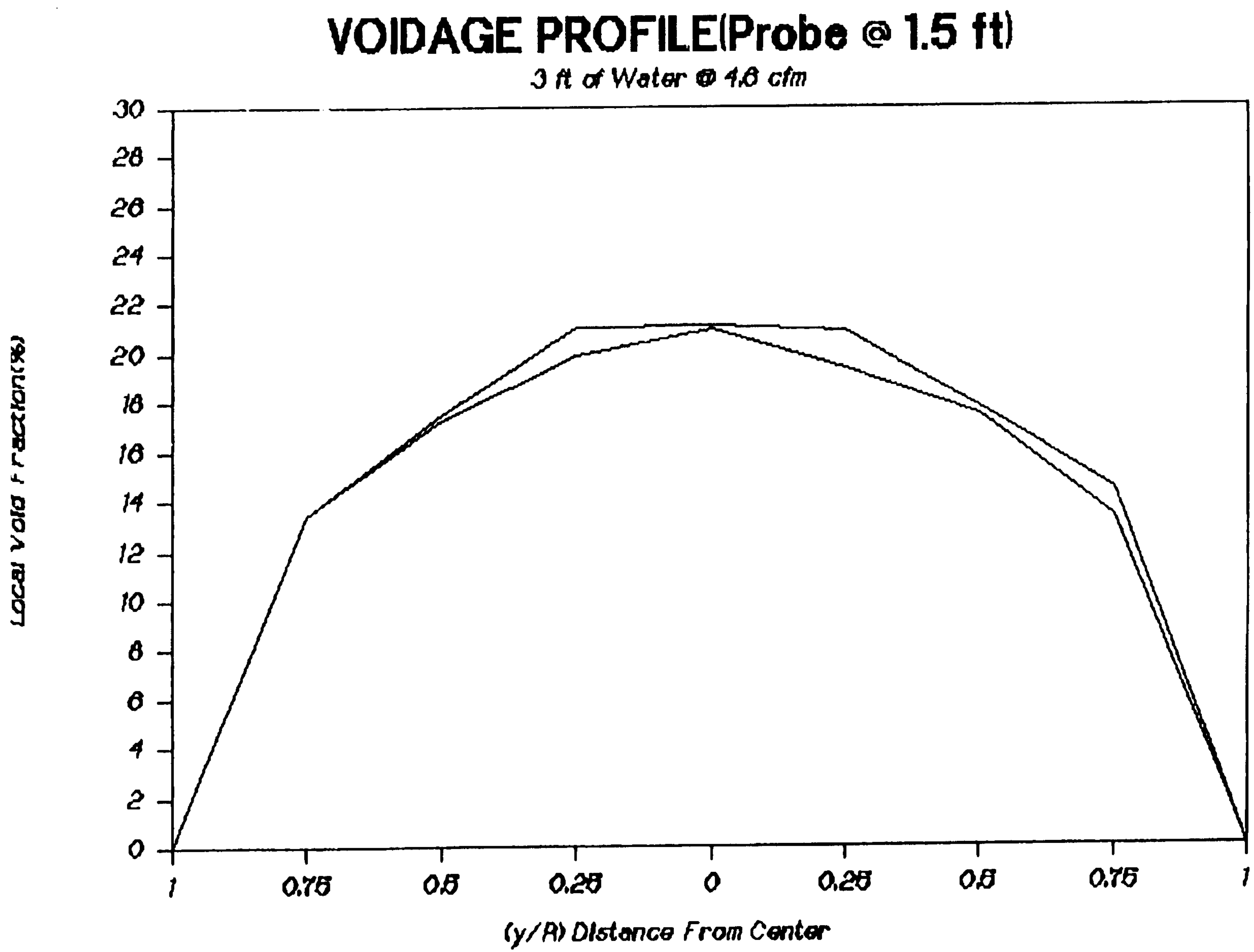

Figure 2.19 Voidage Profile at 18" (3 ft. of water and Q_g = 4.6 CFM)

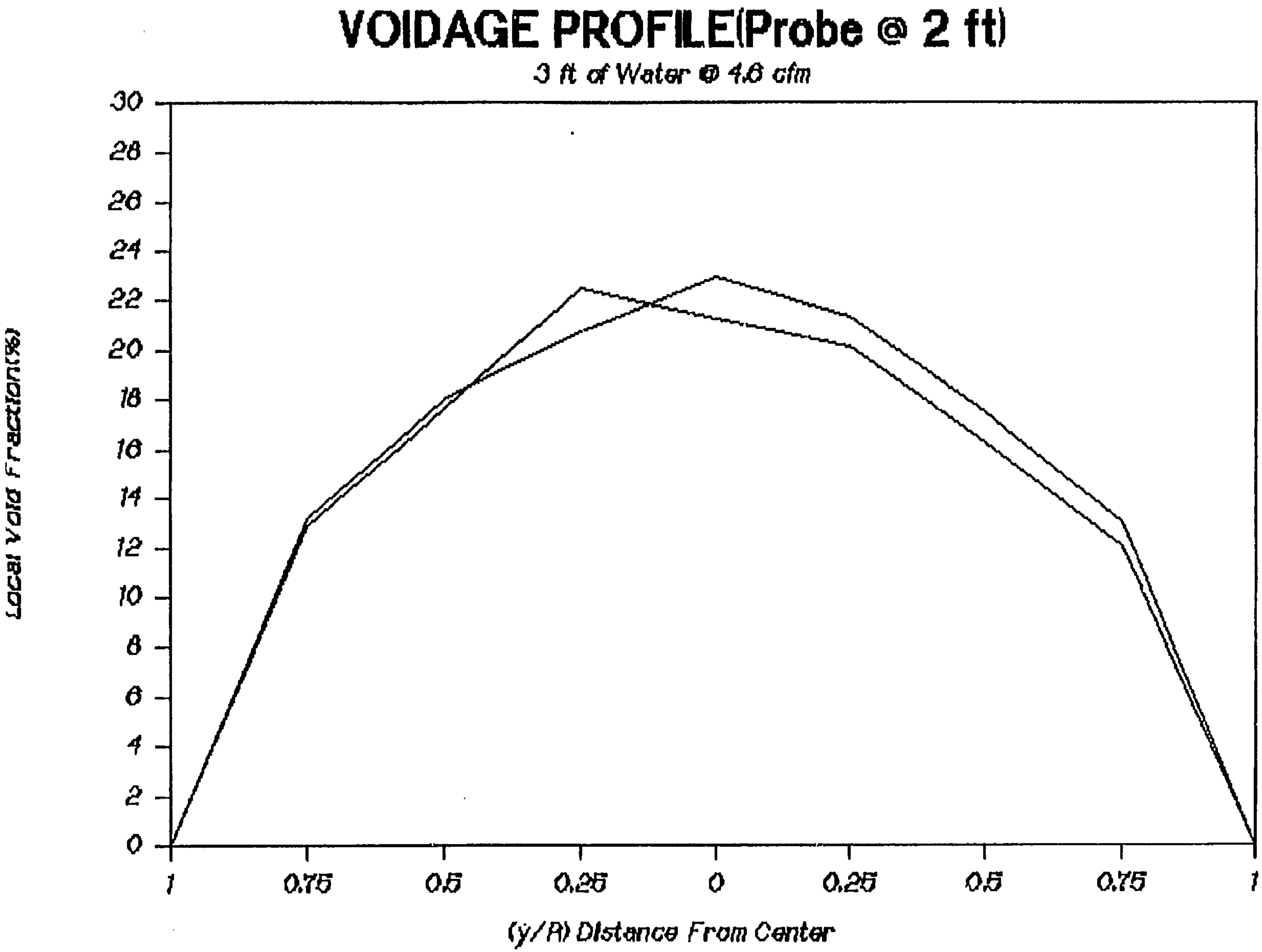

Figure 2.20 Voidage Profile at 24" (3 ft. of water and Q_g = 4.6 CFM)

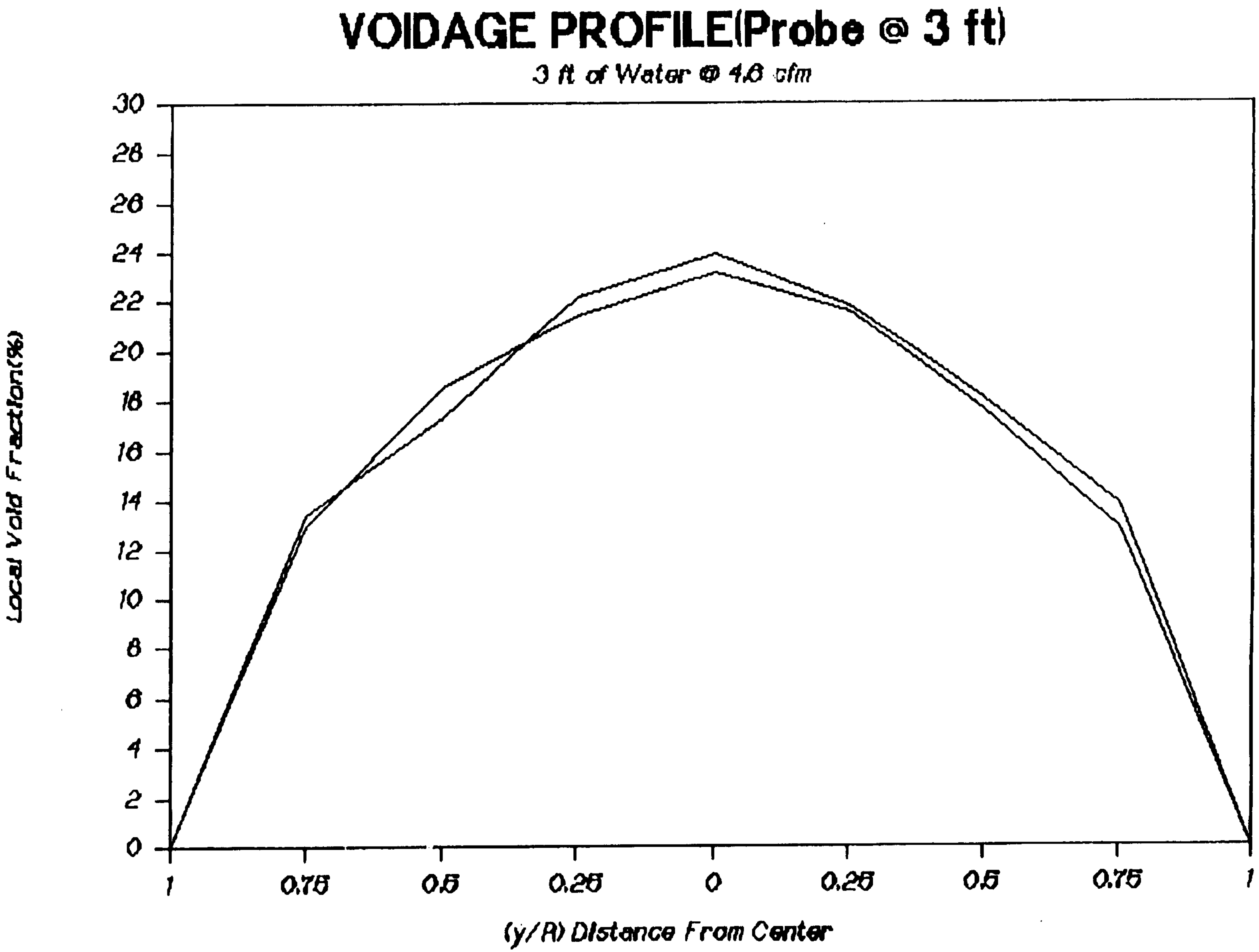

Figure 2.21 Voidage Profile at 36" (3 ft. of water and Q_g = 4.6 CFM)

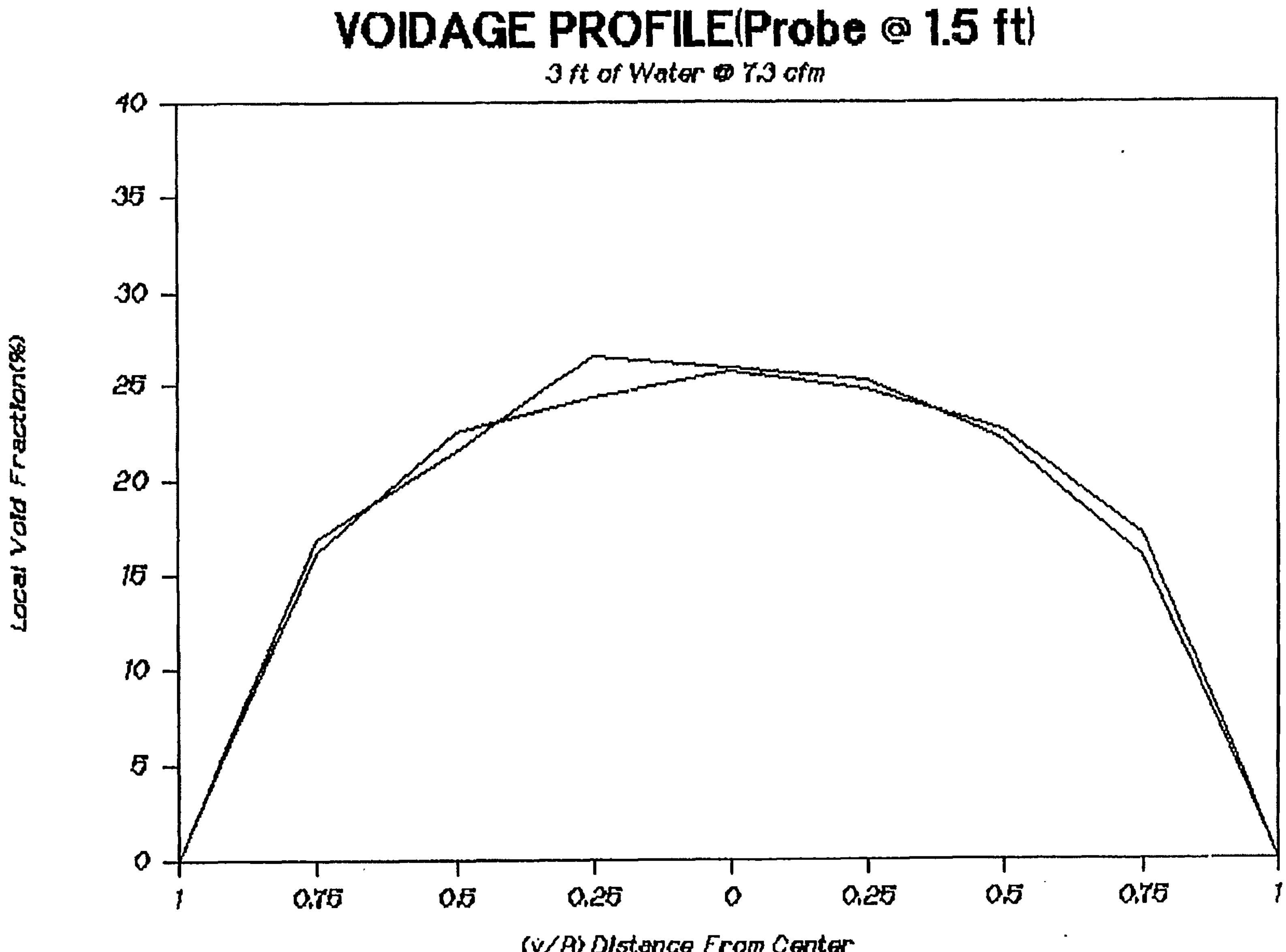

Figure 2.22 Voidage Profile at 18" (3 ft. of water and Q_g = 7.3 CFM)

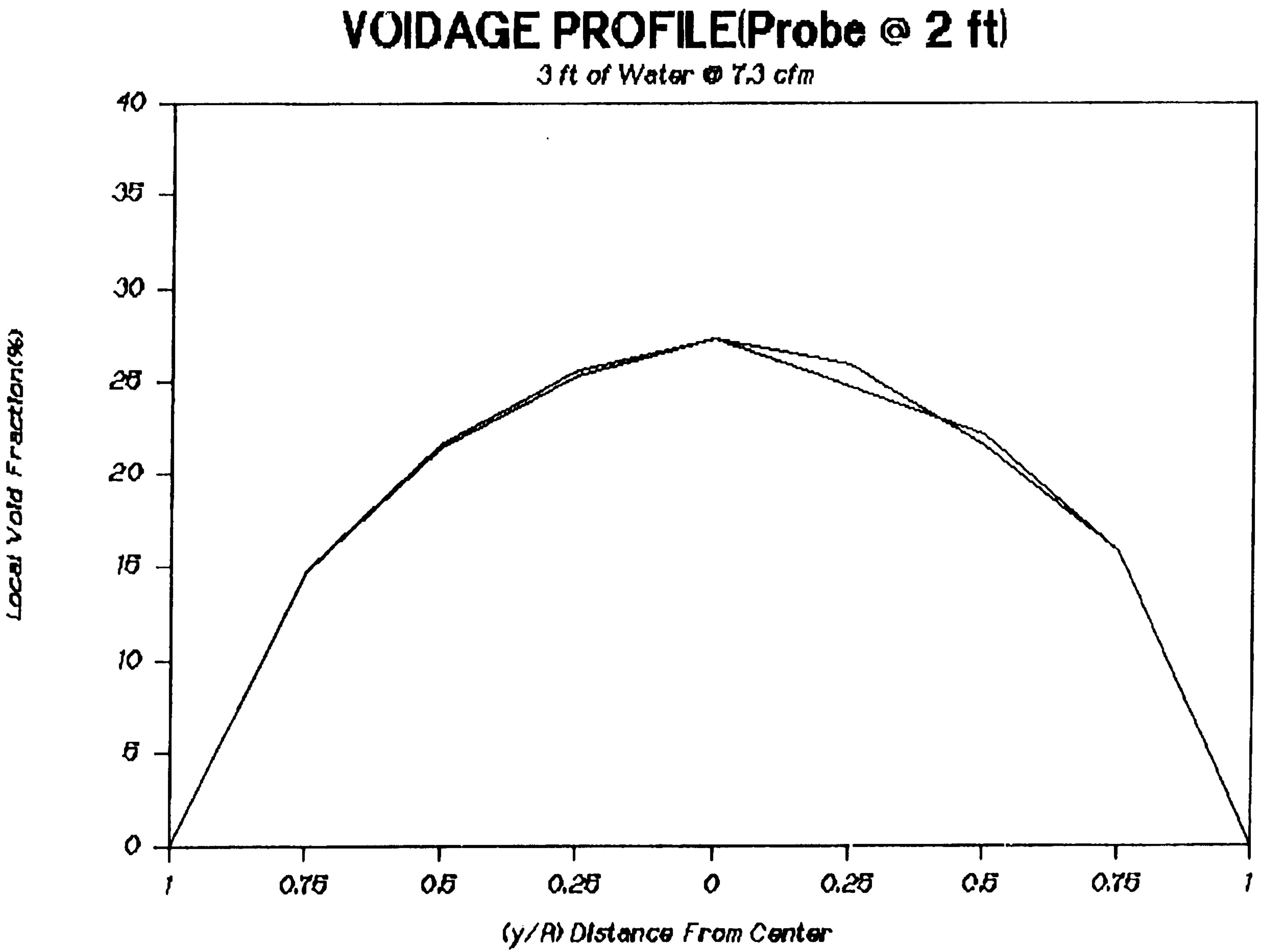

Figure 2.23 Voidage Profile at 24" (3 ft. of water and Q_g = 7.3 CFM)

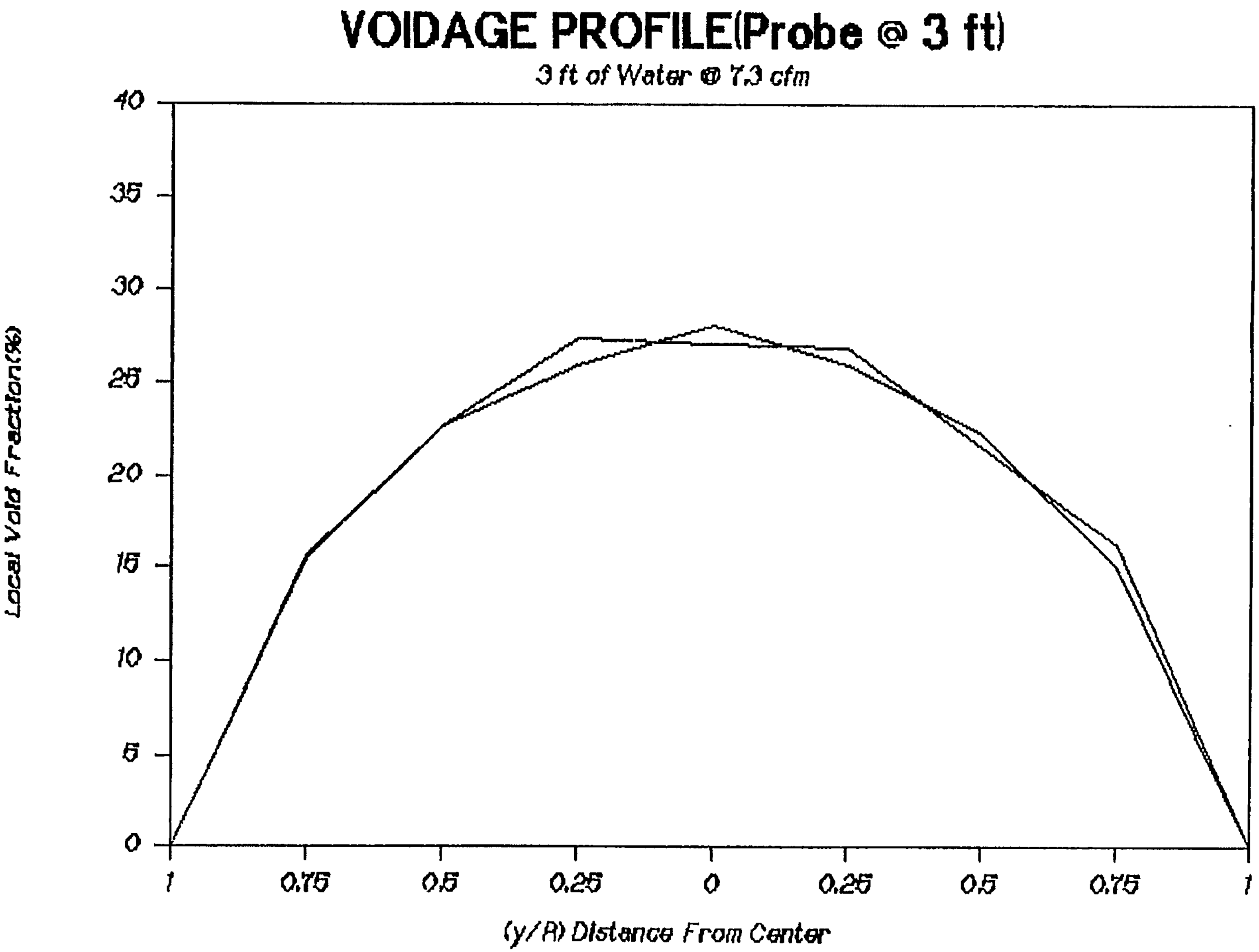

Figure 2.24 Voidage Profile at 36" (3 ft. of water and Q_g = 7.3 CFM)

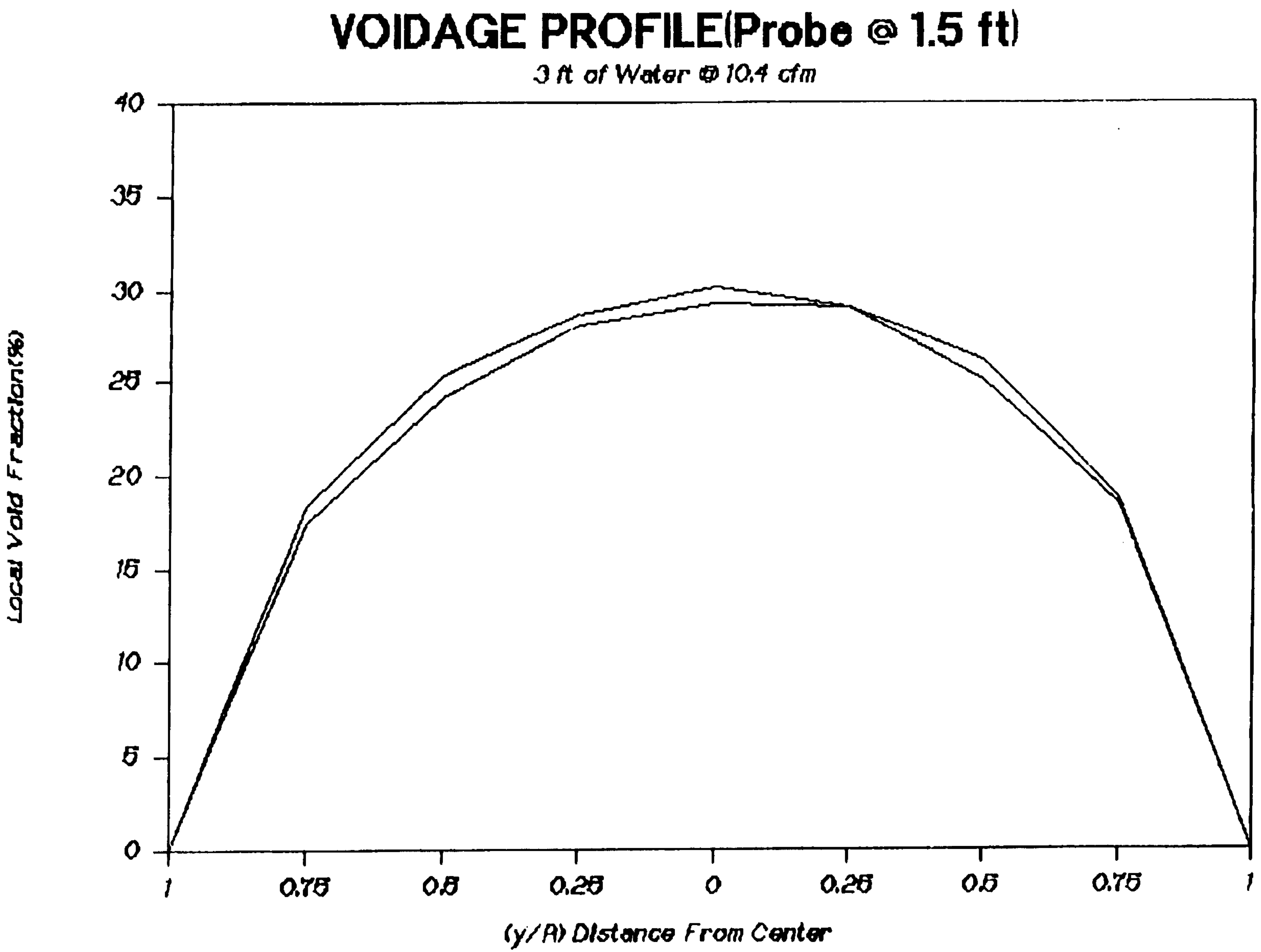

Figure 2.25 Voidage Profile at 18" (3 ft. of water and Q_y = 10.4 CFM)

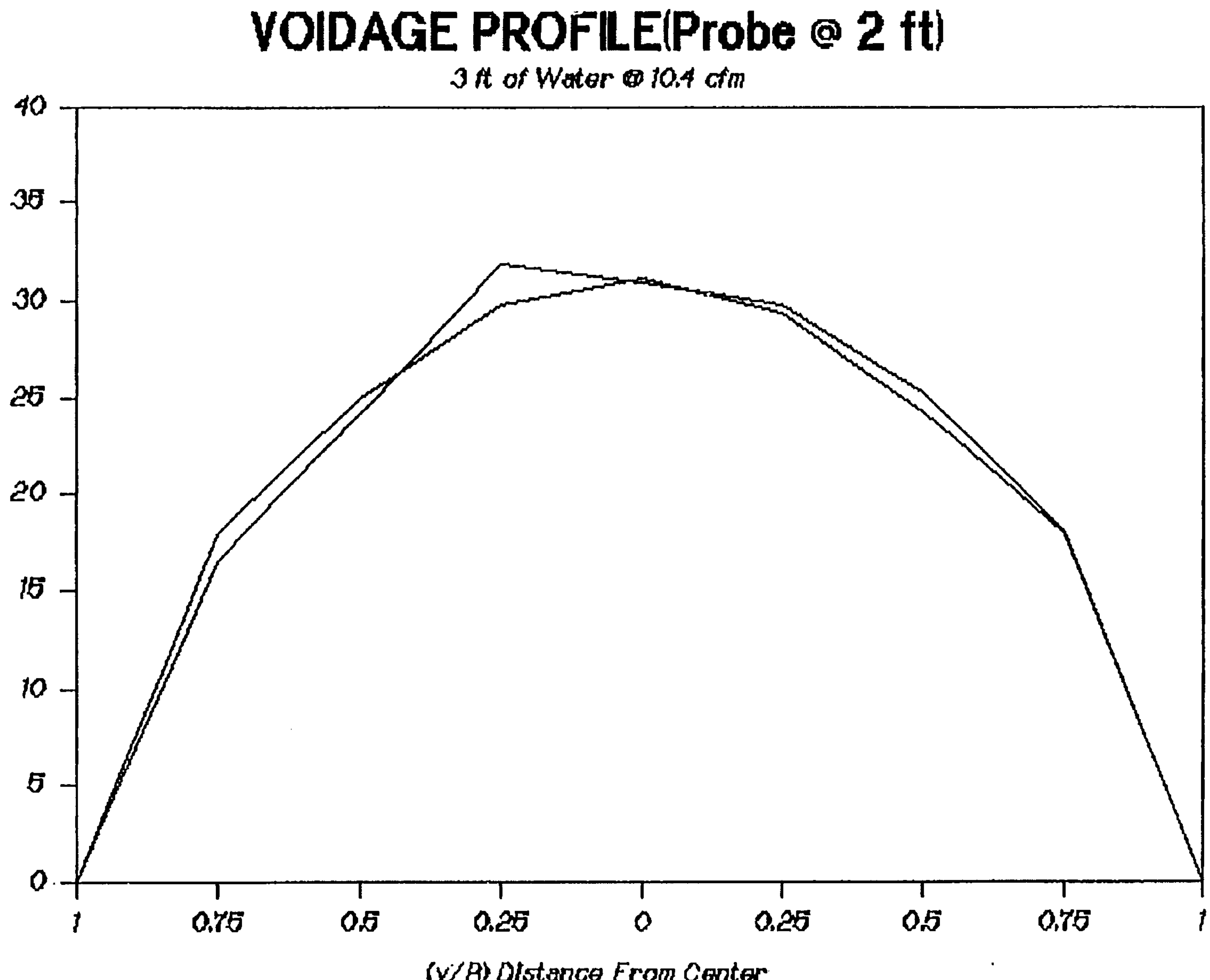

Figure 2.26 Voidage Profile at 24" (3 ft. of water and Q_g = 10.4 CFM)

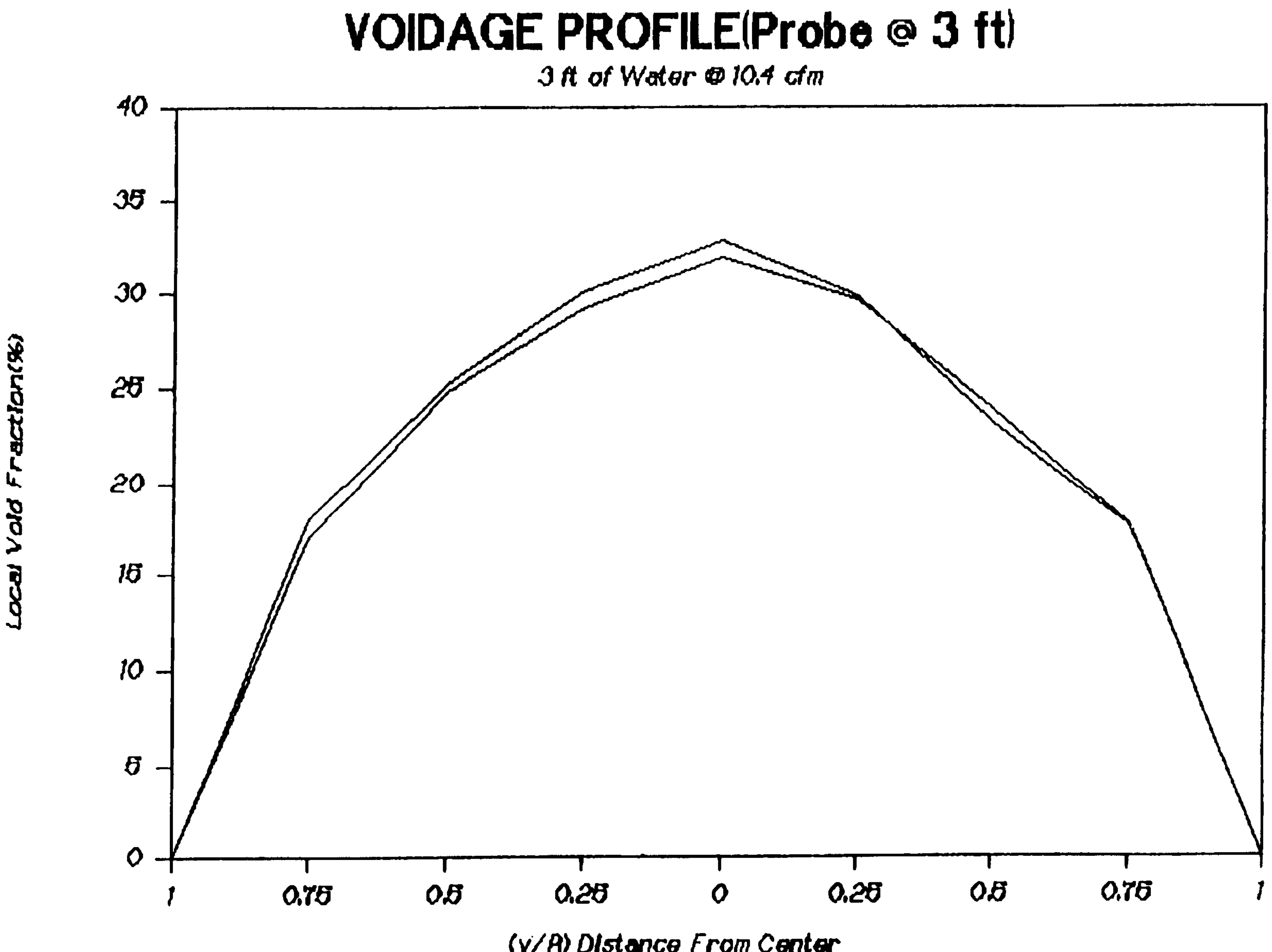

Figure 2.27 Voidage Profile at 36" (3 ft. of water and Q_g = 10.4 CFM)

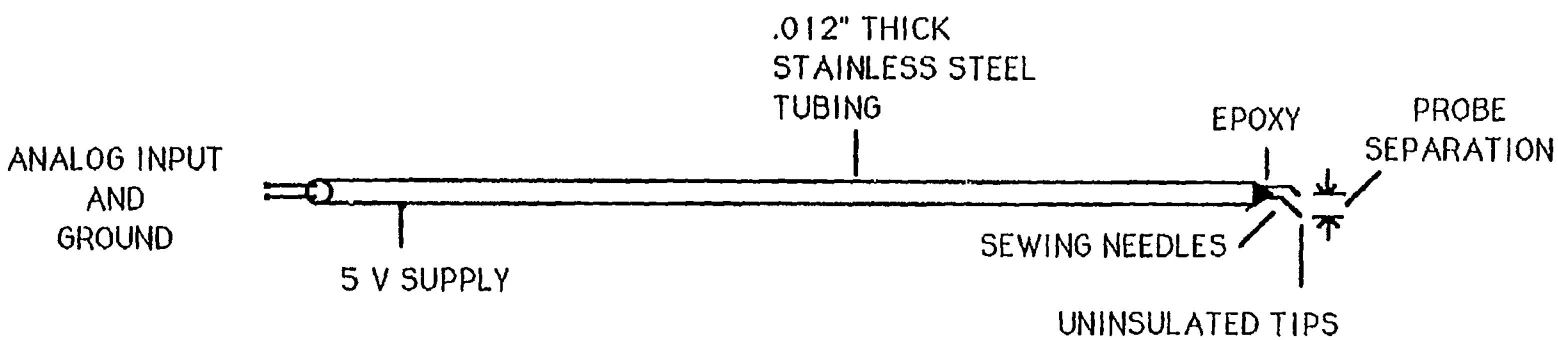

Figure 2.28 Resistance probes for cross-correlation

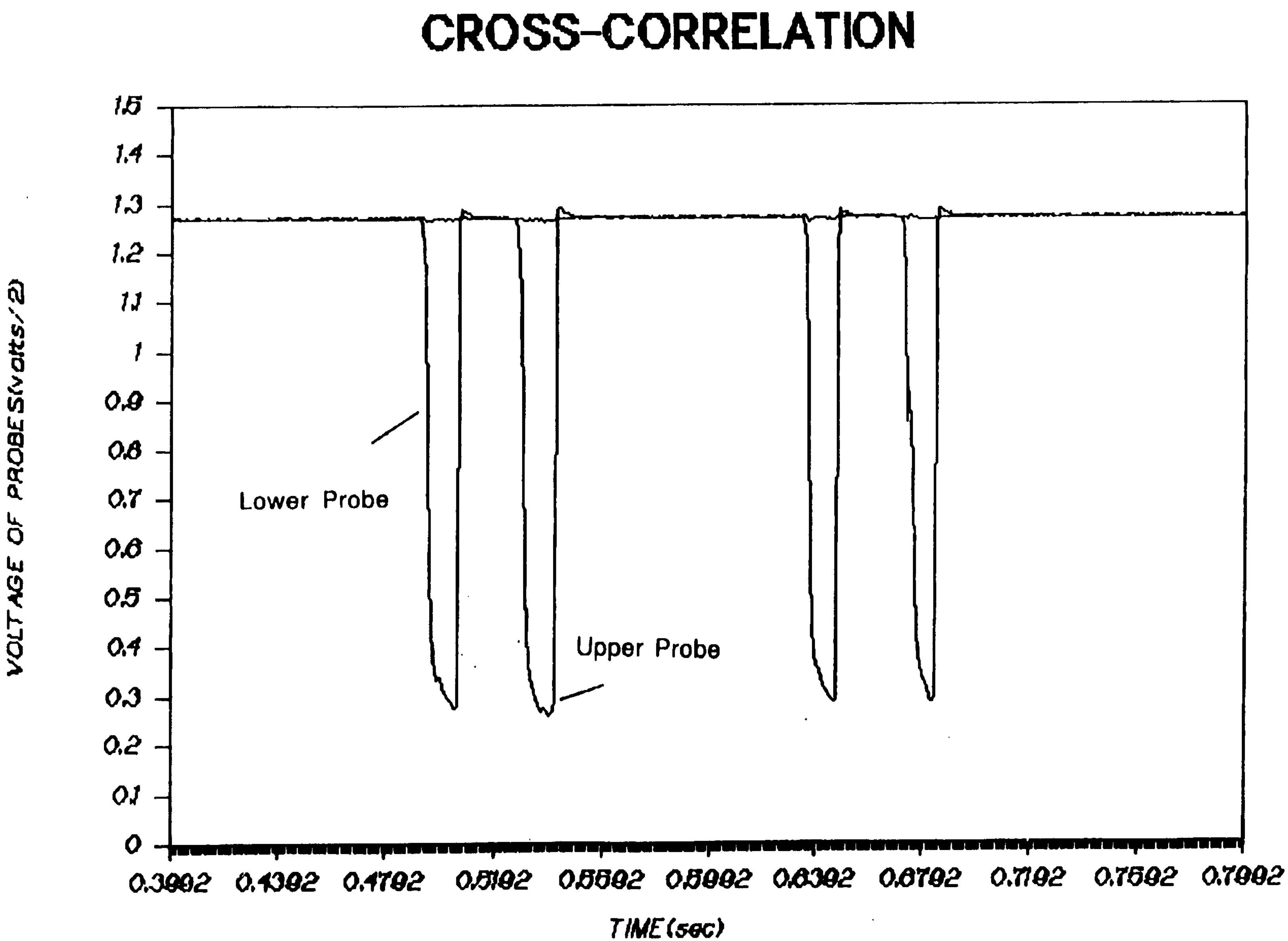

Figure 2.29 Experimental trace from cross-correlation probes

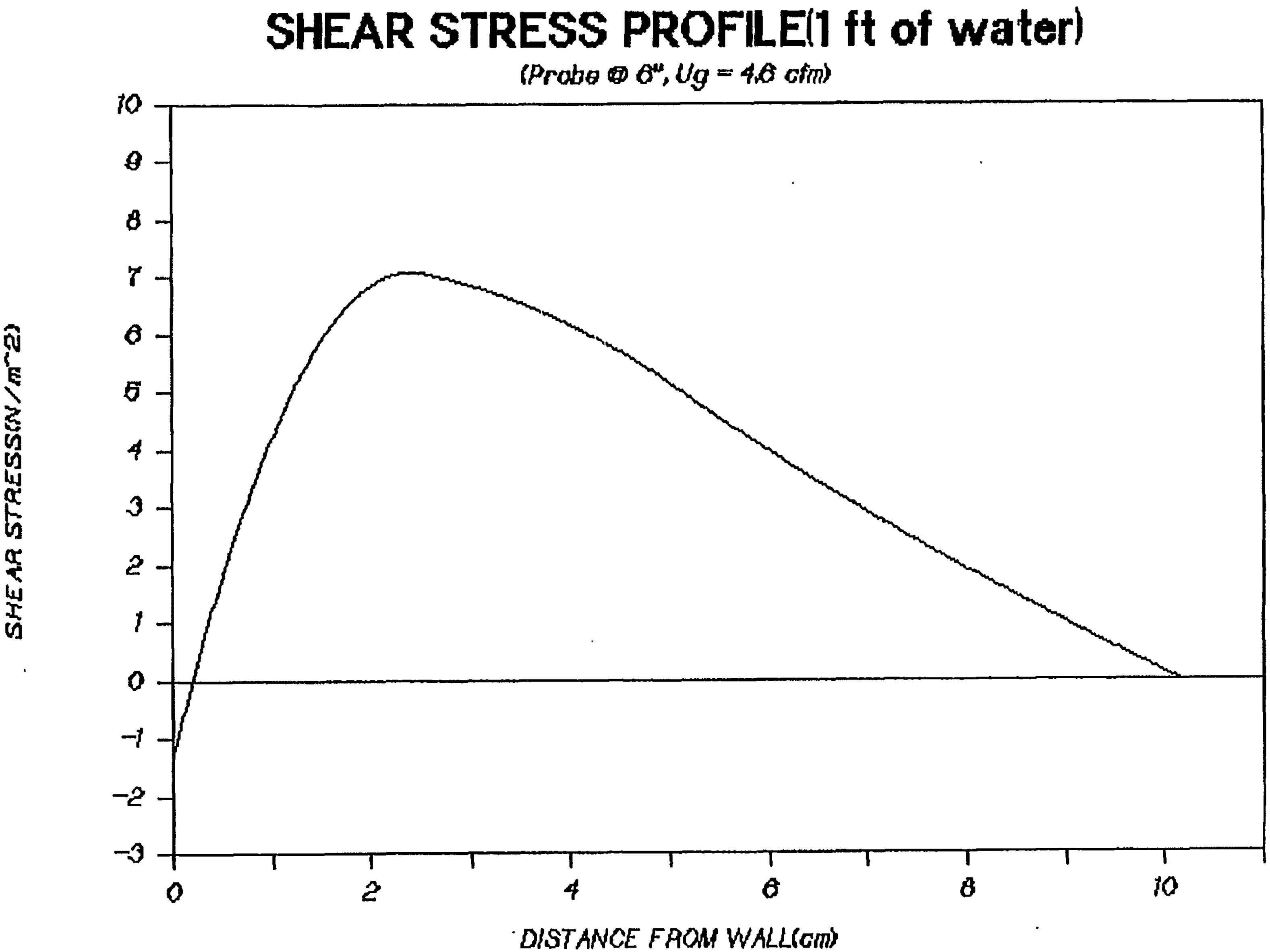

Figure 2.30 Shear stress profile at 6" (1 ft. of water and Q_g = 4.6 CFM)

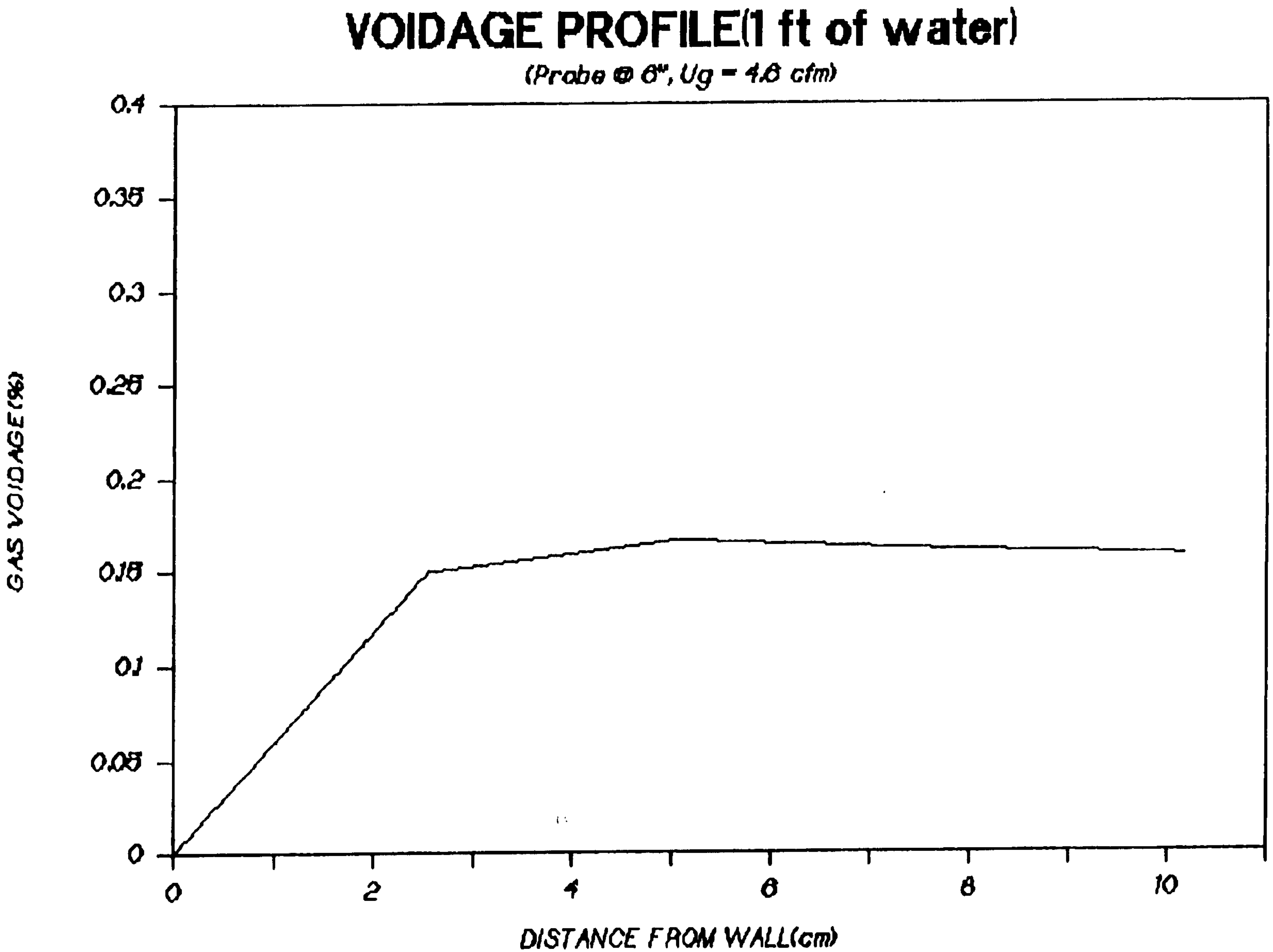

Figure 2.31 Voidage profile at 6" (1 ft. of water and Q_g = 4.6 CFM)

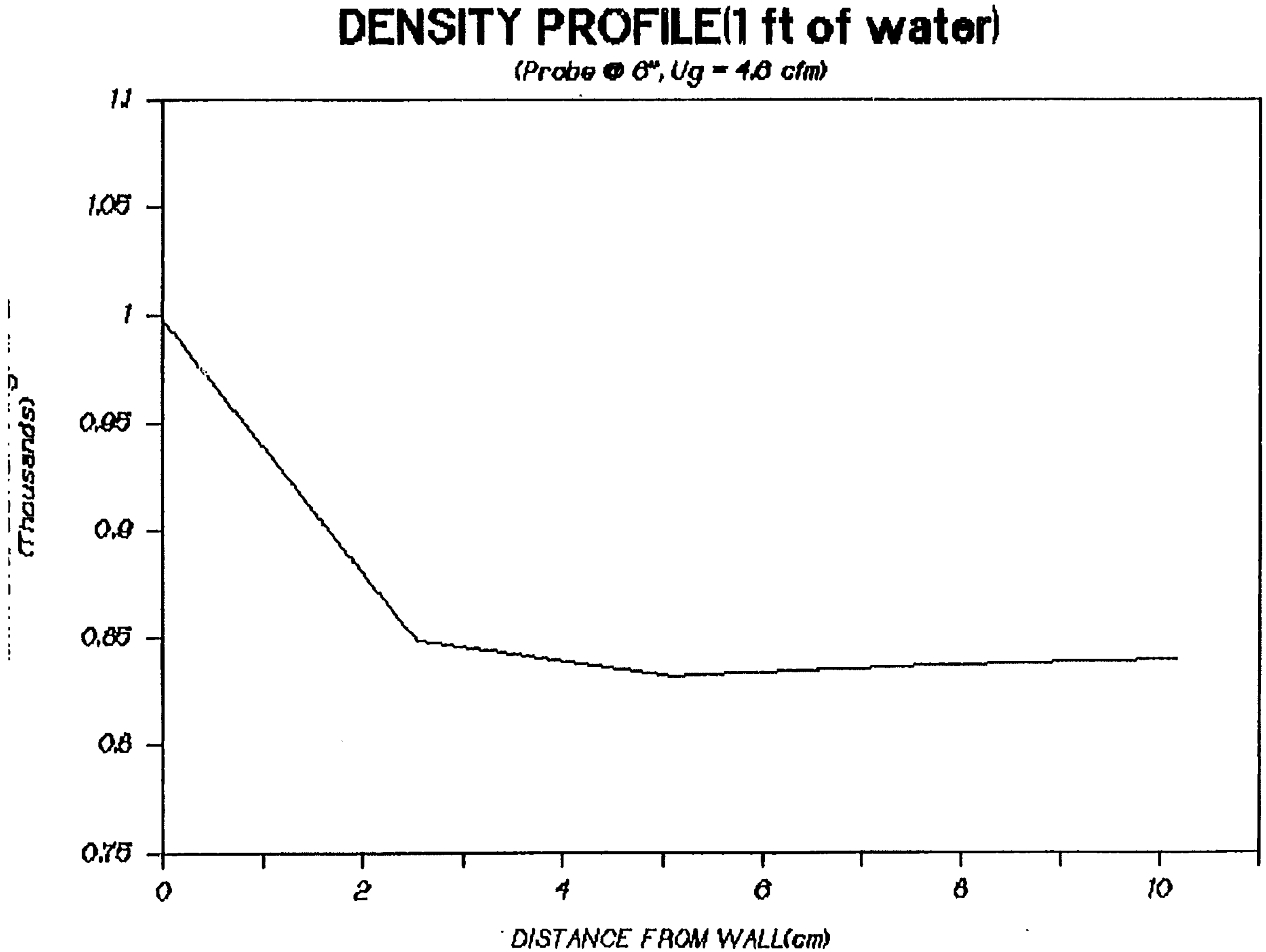

Figure 2.32 Mixture density profile at 6" (1 ft. of water and Q_g = 4.6 CFM)

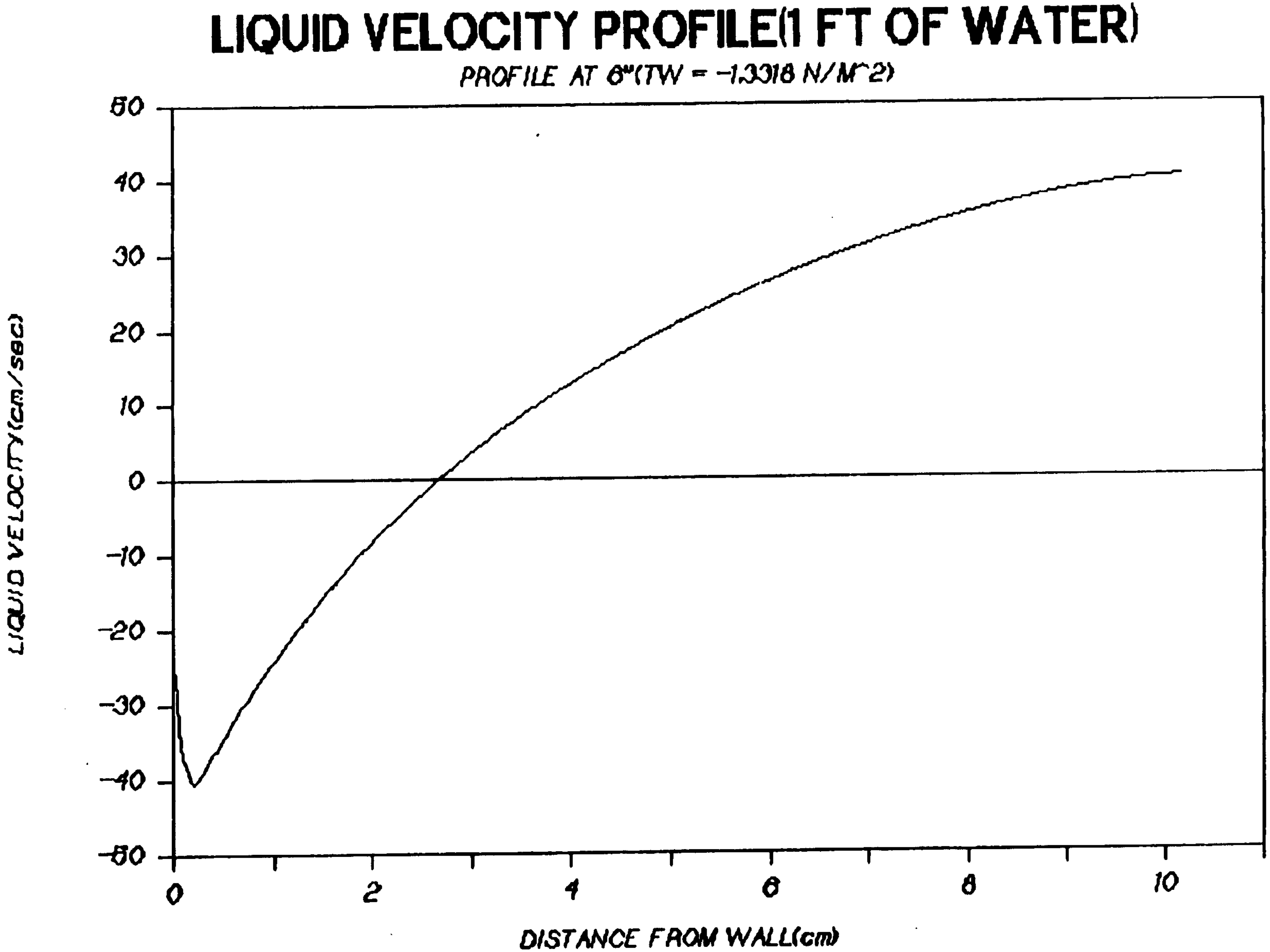

Figure 2.33 Liquid velocity profile at 6" (1 ft. of water and Q_g = 4.6 CFM)

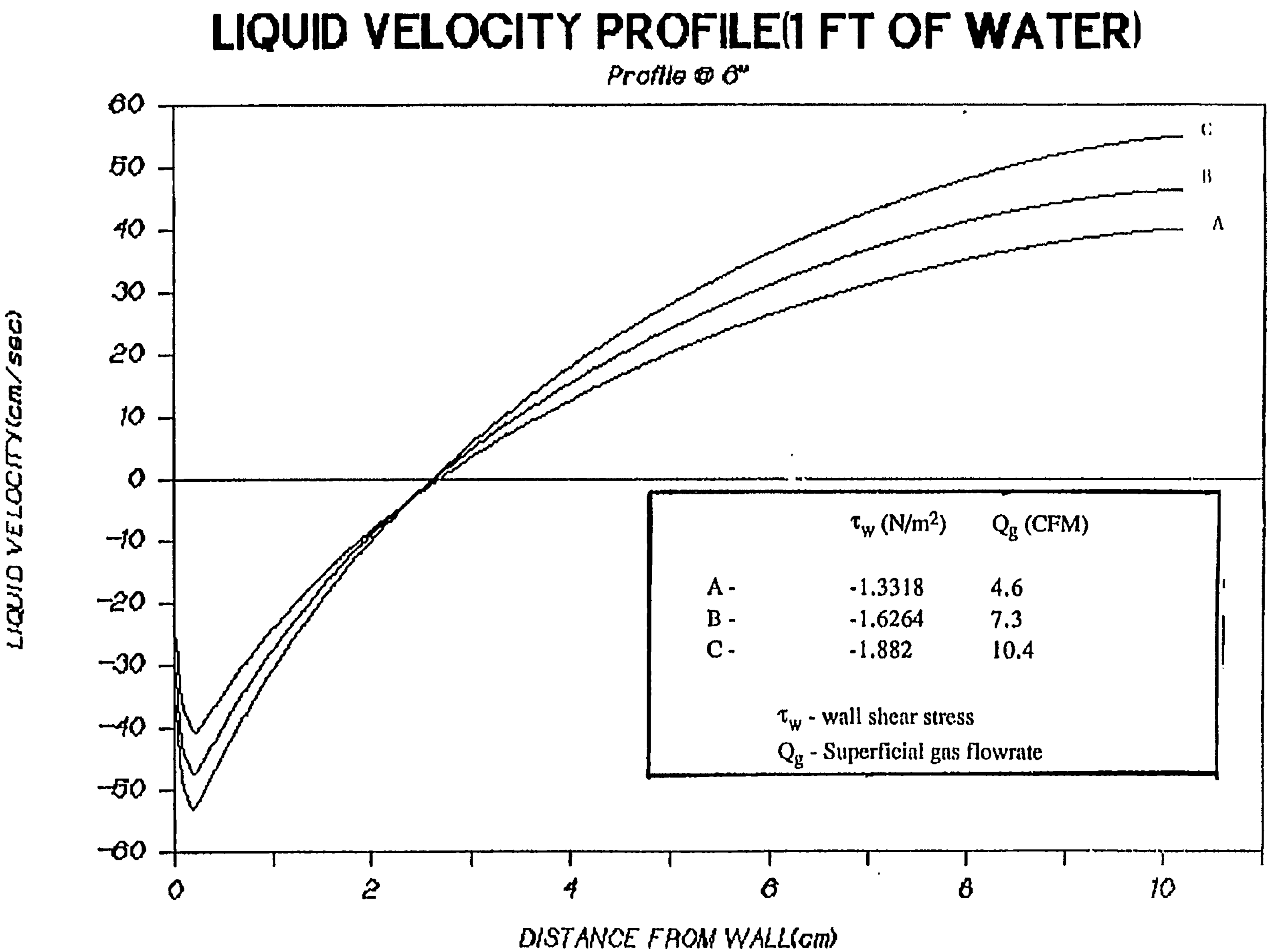

Figure 2.34 Liquid velocity profile at 6" (1 ft. of water at 3 flowrates)

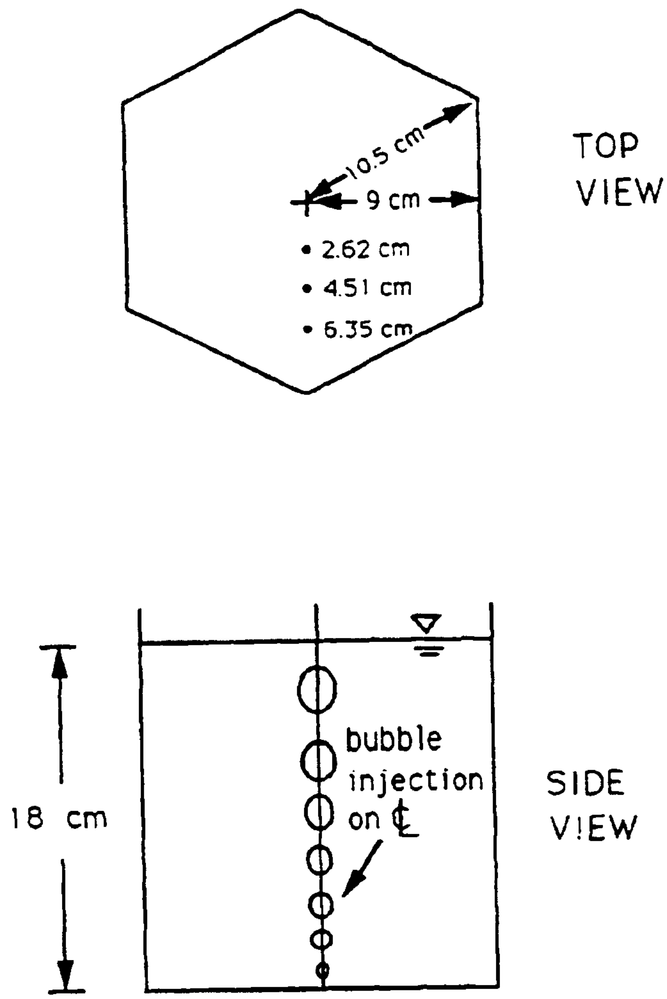

Figure 3.1 Schematic of hexagonal cross-section bubble column for laser doppler velocimeter measurements.

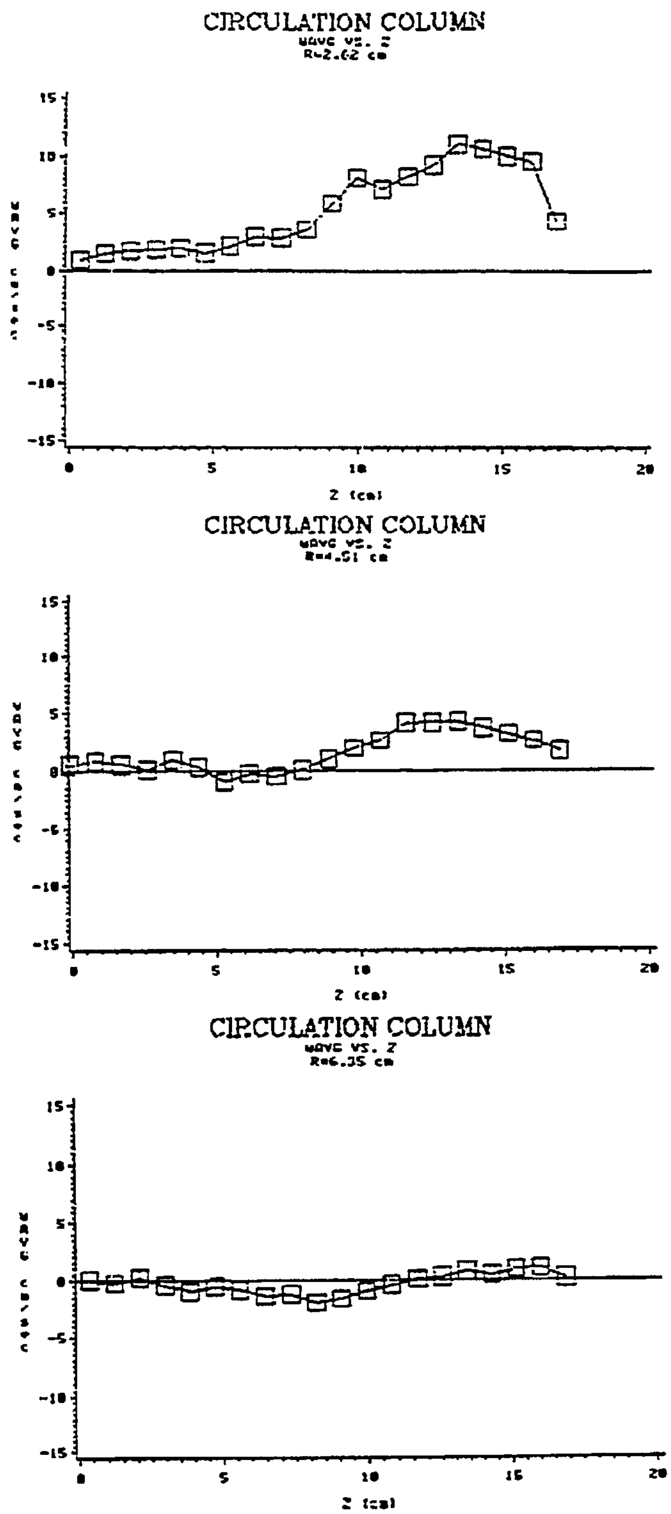

Figure 3.2 Preliminary measured mean vertical velocity profiles in hexagonal bubble column versus depth at three different radii; air flow rate = 2 SCFH.

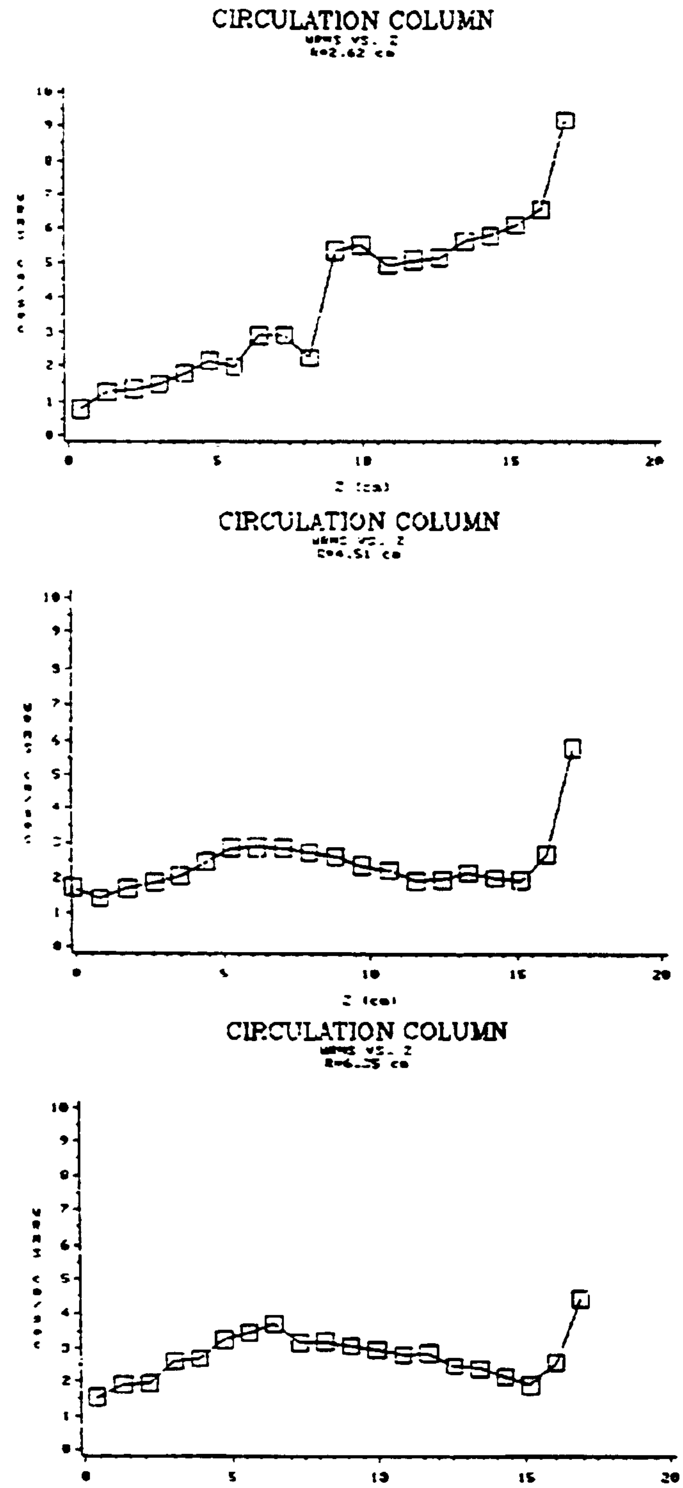

Figure 3.3 Preliminary measured RMS vertical velocity profiles in hexagonal bubble column versus depth at three different radii; air flow rate = 2 SCFH.

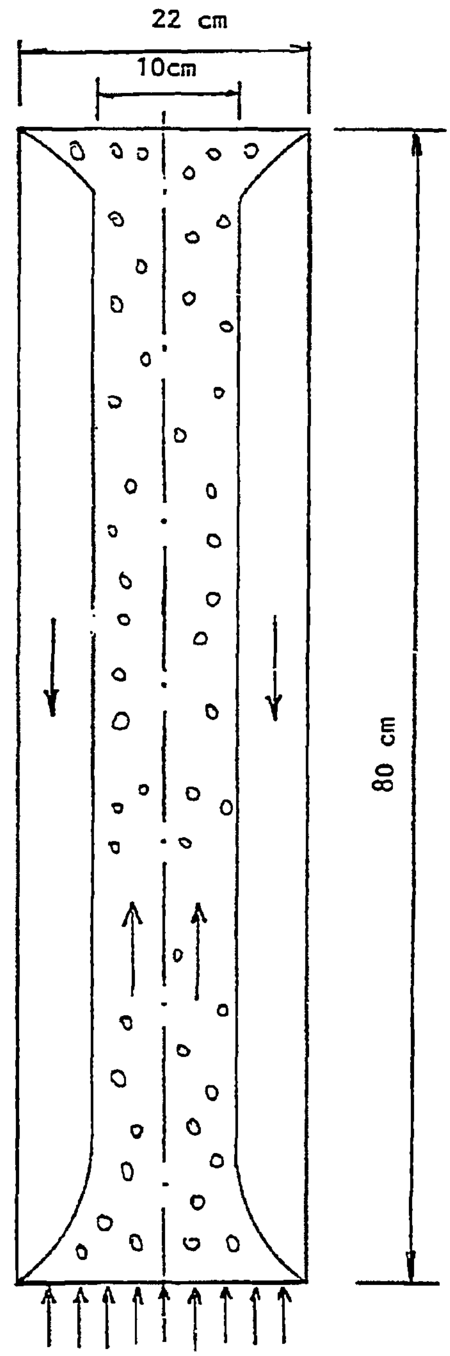

Fig. 4.1 Geometry of the bubble column

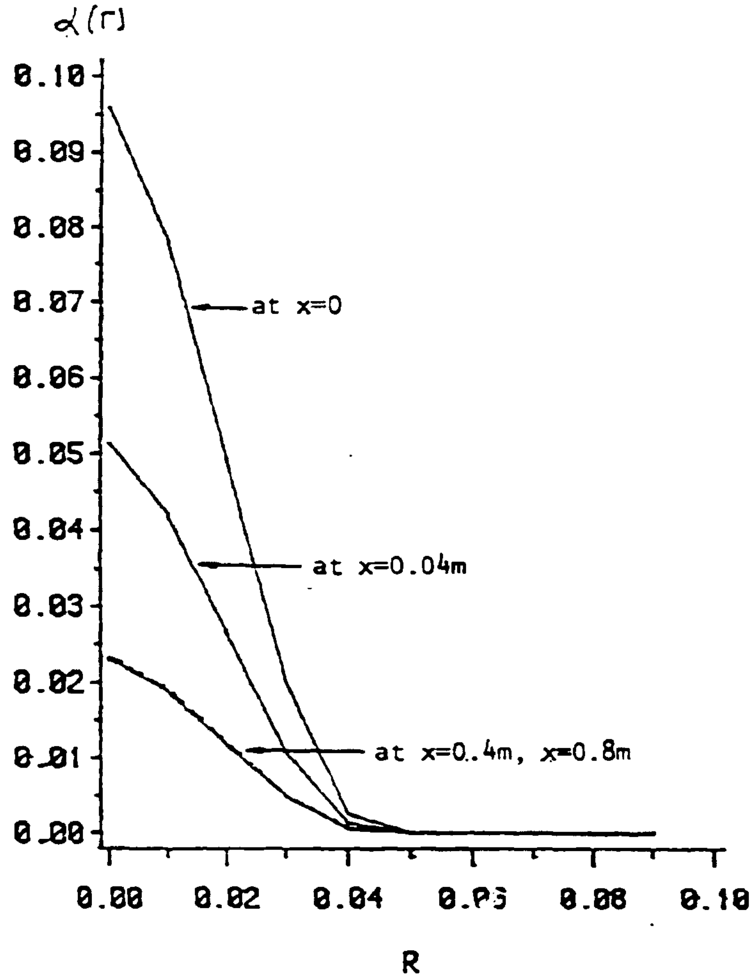

Fig. 4.2 Void fraction distribution as a function of the radial distance

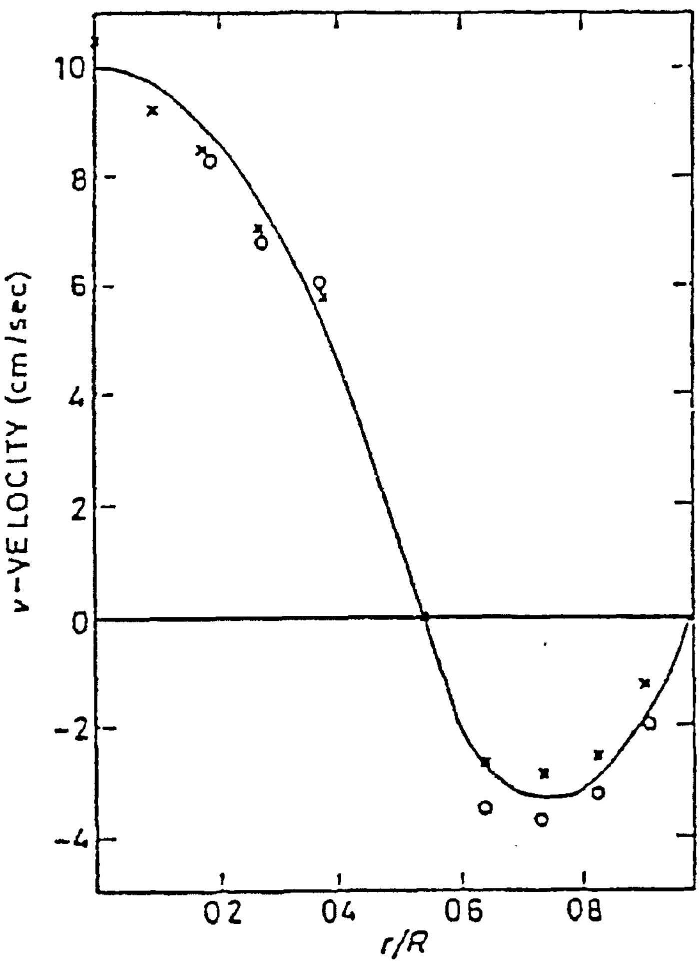

$q_d = 0.3834\times10^{-6}$ $\quad$ $\varepsilon = 0.0118$

$\phi = 0.4108\times10^{-4}$ $\quad$ $\delta = 0.46$

Fig. 4.3 Experimentally determined velocity profile, from Rietema and Ottengraf (1970).

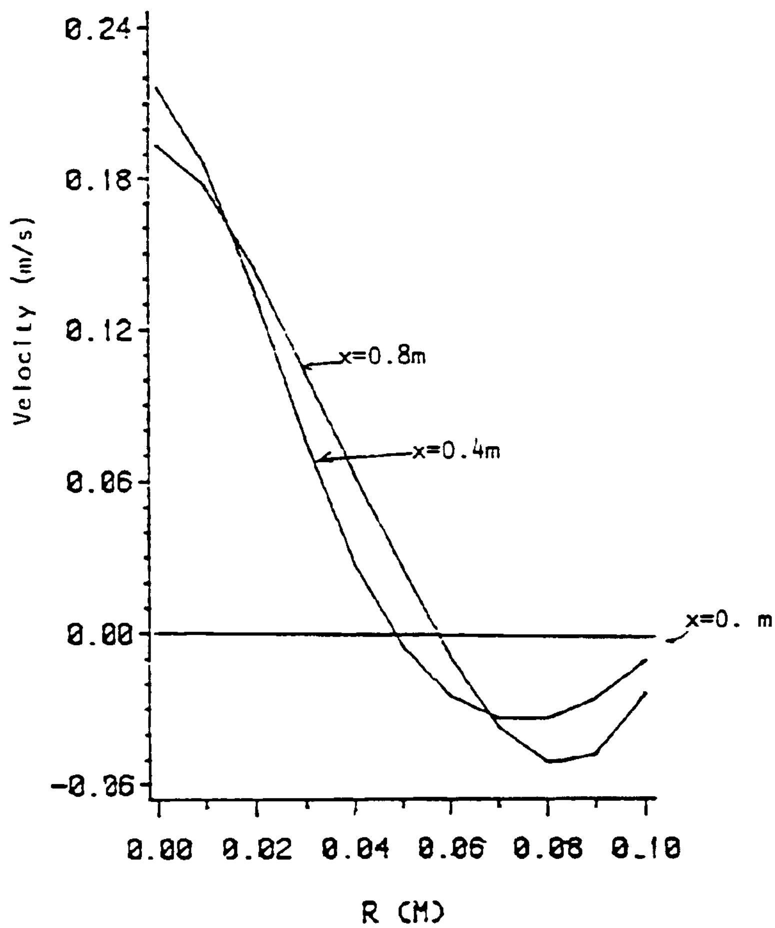

Fig. 4.4 Calculated Liquid Velocity Profiles

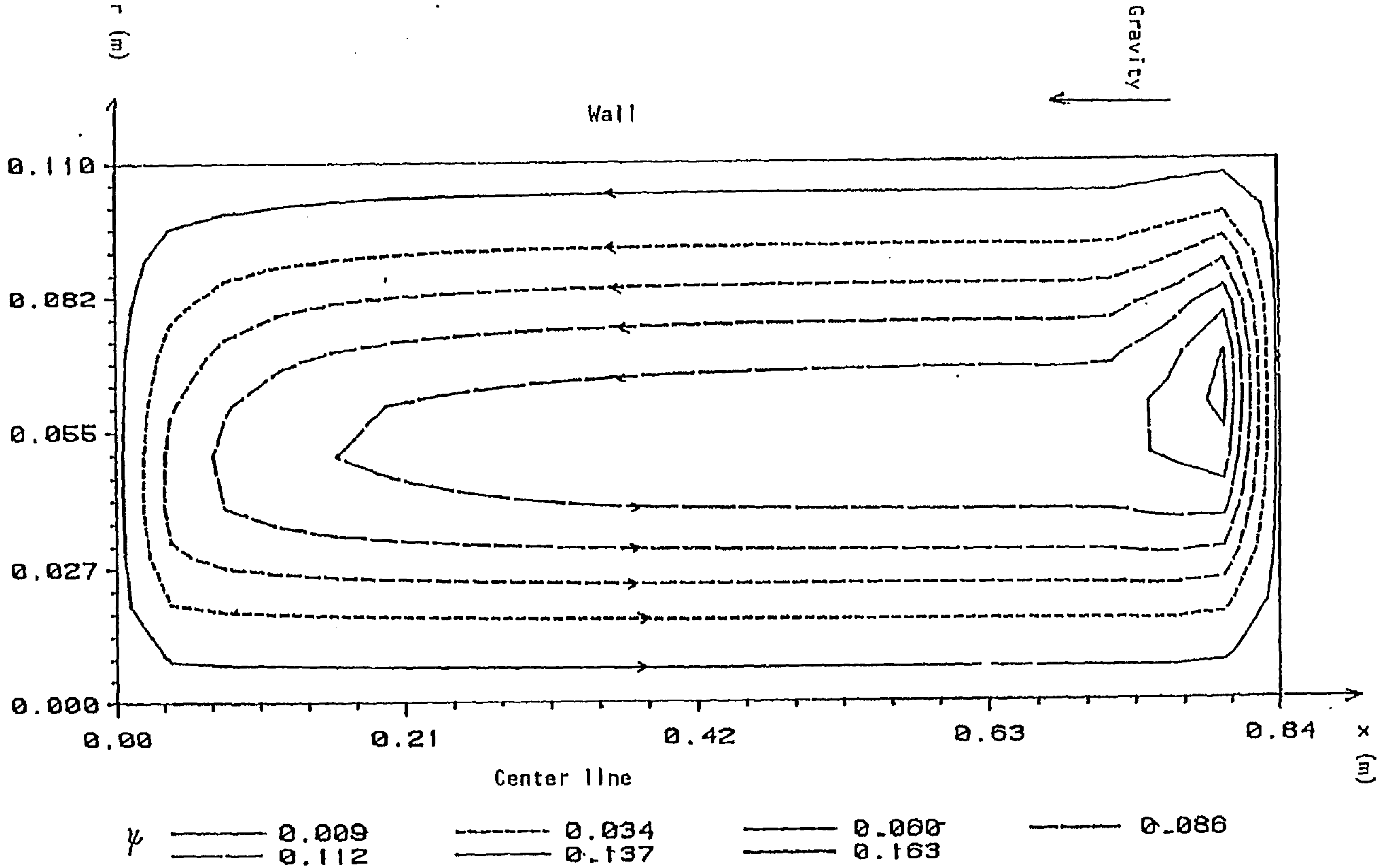

Fig. 4.5 Liquid phase stream line contours

APPENDIX A Cross-Correlation Program

```
1     DEFINT A-Y
      DEFSNG Z
        DIM ARRAY(16000), ZA(301), ZV(11)
      FOR KK = 1 TO 10
50    ERSTAT = 0
        CALL INITIALIZE(ERSTAT)
        IF ERSTAT = 0 THEN 100
          PRINT "THE ERROR IS"; ERSTAT
          INPUT Q$
          GOTO 1
100   LCHAN = 1
        BOARD = 1
        ERSTAT = 0
        PCHAN = 0
        MULT = 50
        RANGE = 10
        COUNT = 16000
        GAIN = 1
        CALL SCAN515(LCHAN, BOARD, PCHAN, RANGE, MULT, COUNT, GAIN, ERSTAT)
        IF ERSTAT = 0 THEN 200
          PRINT "THE ERROR IS"; ERSTAT
          INPUT Q$
          GOTO 100
200   INPUT "COLLECTION OF DATA BEGINS ON ANY INPUT"; B$
        PRINT TIMER
        LCHAN = 1
        ERSTAT = 0
          CALL SCAN(LCHAN, ARRAY(1), ERSTAT)
        IF ERSTAT = 0 THEN 300
          PRINT "THE ERROR IS"; ERSTAT
          INPUT Q$
          GOTO 200
300   LCHAN = 1
        ERSTAT = 0
310   CALL CHECK(LCHAN, ERSTAT)
        IF ERSTAT = 117 THEN 400
          GOTO 310
400   PRINT "COLLECTION OF DATA COMPLETE"
      PRINT TIMER
      READ A$
        OPEN "O",#1,A$
        FOR I = 1 TO COUNT
          PRINT #1,ARRAY(I)
        NEXT I
        CLOSE #1
         FOR K = 1 TO 151
          L = K - 51
          ZA(K) = 0
          IF K <= 51 THEN GOTO 500
          M = COUNT - 201
          N = 1
          FOR I = N TO M STEP 2
            ZA(K) = ZA(K) + ((ARRAY(I)/2)*(20/4096)) * ((ARRAY(I + 2 * L + 1)/2)*(20/4096))
          NEXT I
          GOTO 500
```

```
500     N = 1 + 200
        M = COUNT - 1
        FOR I = N TO M STEP 2
          ZA(K) = ZA(K) + ((ARRAY(I)/2)*(20/4096)) * ((ARRAY(I + 2 * L + 1)/2)*(20/4096))
        NEXT I
600     NEXT K
       T = 0
       TEMP = 0
       FOR I = 1 TO 151
         IF ZA(I) < TEMP THEN GOTO 650
           TEMP = ZA(I)
           ZV(LL) = I
650    NEXT I
       IF ZV(LL) > 51 THEN 700
         ZV(LL) = 51 - ZV(LL)
         GO TO 750
700    ZV(LL) = ZV(LL) - 51
750   NEXT JK
      DATA "RAWDATA"
      END
```

U.S. DEPARTMENT OF COMMERCE
Technology Administration
National Technical Information Service
Springfield, VA 22161 (703) 605-6000